ACTINIDE RESEARCH QUARTERLY

Ac Th Pa U Np Pu Am Cm Bk Cf Es Fm Md No Lr

Second Quarter 2019

PLUTONIUM FUTURES 2018 CONFERENCE ISSUE

NUMBER 1 OF 2

Los Alamos
NATIONAL LABORATORY
EST. 1943

Foreword

"Plutonium Futures—The Science 2018" was the tenth in a series of international conferences focused on the scientific research and technological uses of plutonium and other actinides. The global actinide research and technology community takes great pride in this series as its origins lie in the United Nations "Peaceful Uses of Atomic Energy" conference series initiated in 1958. Co-organized by Los Alamos National Laboratory (LANL), Lawrence Livermore National Laboratory (LLNL), and the American Nuclear Society, and supported by the U.S. Department of Energy and the National Nuclear Security Administration (NNSA), Plutonium Futures—The Science 2018 was held at the Wyndham San Diego Bayside, September 9–14, 2018. A total of 218 attendees from around the world participated in talks and discussions—many of these topics presented at Plutonium Futures resonate with those found in the early days of international cooperation. This conference facilitates dialogue among scientists and engineers of diverse scientific disciplines on the science of plutonium and its technological, environmental, health, and socio-economic consequences.

This issue of the LANL Actinide Research Quarterly is the first of two issues celebrating the breadth of topics presented at last year's conference, including: environmental chemistry, metallurgy and materials science, surface science and corrosion, coordination chemistry, nuclear fuel-cycle, detection and speciation analysis, and condensed matter physics. The articles here represent many of the stimulating pieces of research conducted by the global actinide research and technology community. In the tradition of the Plutonium Futures conferences, we recognize here the best student posters (*p25*). We would also like to recognize the various committees which assisted in organizing and conducting Plutonium Futures—The Science 2018, listed on the facing page.

— Franz Freibert, Co-Chair Plutonium Futures 2018

Plutonium Futures 2018 Committees:
Los Alamos National Laboratory
Franz Freibert Co-chair
Albert Migliori Co-chair
Susan Ramsay Conference Coordinator
David Clark
Andrew Gaunt
George Goff
Sarah Hernandez
John Joyce
Stosh Kozimor
Boris Maiorov
Stuart Maloy
Jeremy Mitchell
David Moore
Dominic Peterson
Don Reed
Blas Uberuaga
Marianne Wilkerson
Ping Yang

Program Committee
Corwin Booth Lawrence Berkeley National Laboratory, LBNL
Paul Roussel Atomic Weapons Establishment, AWE
Sue Ennaceur AWE
Robert J. Hanrahan Jr. NNSA
Benoit Oudot CEA Valduc
David Hobart Florida State University
Klaus Luetzenkirchen DG Joint Research Centre JRC
Richard Wilson Argonne National Laboratory
David Shuh LBNL
Krzysztof Gofryk Idaho National Laboratory
Philippe Moisy CEA Marcoule
Rudy Konings JRC
Mavrik Zavarin LLBL
Stepan Kalmykov Lomonosov Moscow State University
Horst Geckeis Karlsruhe Institute of Technology
John Gibson LBNL

International Advisory Committee
Herve' Bernard CEA
Claude Guet University of Singapore
Gerry Lander Institut Laue-Langevin
Roberto Caciuffo European Commission, JRC
Thomas Fanghänel European Commission, JRC
David Geeson AWE, Aldermaston
Tim Tinsley National Nuclear Laboratory
Gerrit van der Laan Diamond Light Source Ltd.
Kerri Blobaum LLNL
David Clark LANL
Scott McCall LLNL
Rodney C. Ewing Stanford University
Siegfried Hecker Stanford University
Jun Li Tsinghua University
Vladimir Dremov RFNC-VNIITF
Boris Nadykto VNIIEF
V. Petrovtsev RFNC-VNIITF
Lidia F. Timofeeva VNIINM
Yoshinori Haga Japan Atomic Energy Agency
Ladislav Havela Charles University, Prague

Plutonium Futures

The Science 2018

Contents

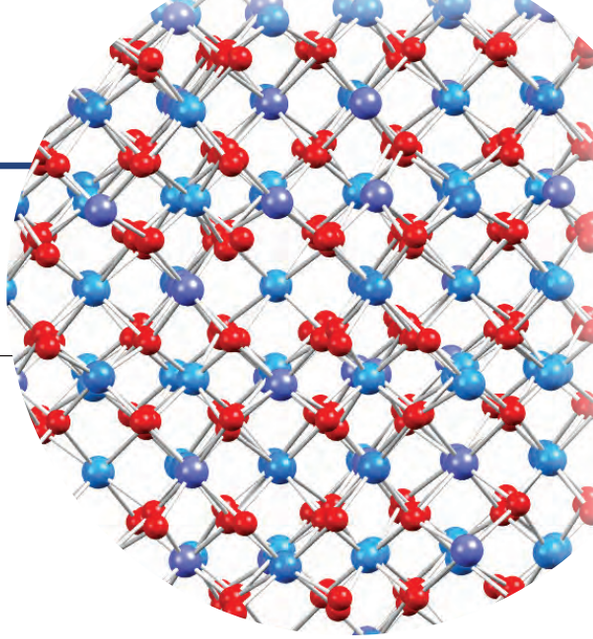

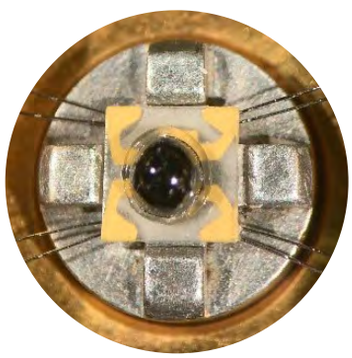

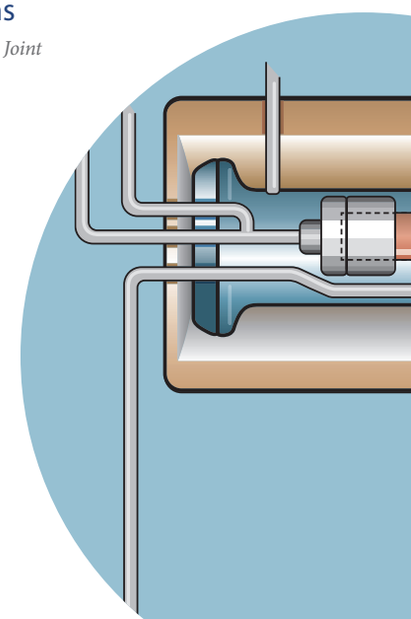

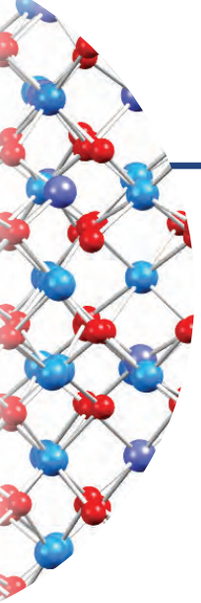

About the cover: The (pressure, temperature) phase diagram of elemental plutonium has been a central and long-debated aspect of actinide science. This plot shows unusual behavior, such as the multitude of allotropes or distinct crystallographic phases of elemental plutonium—see *p19* for a more detailed view. The forthcoming second part in the Plutonium Futures conference series (third quater 2019, *right*) will continue with seven more articles adapted from talks during the 2018 meeting.

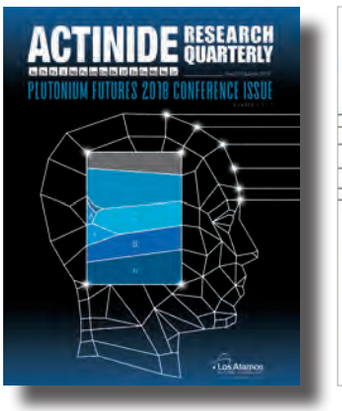

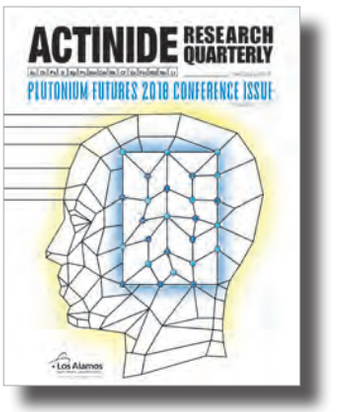

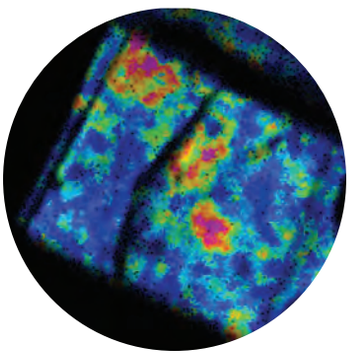

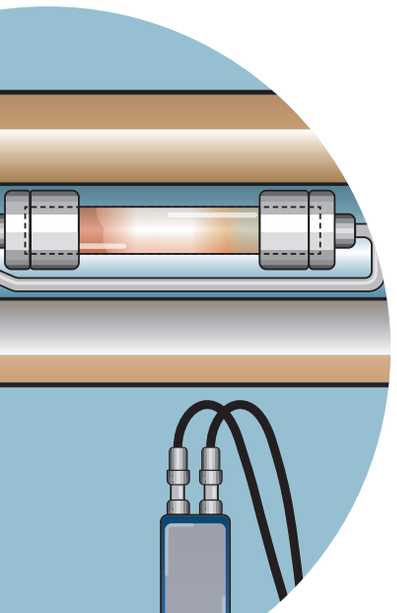

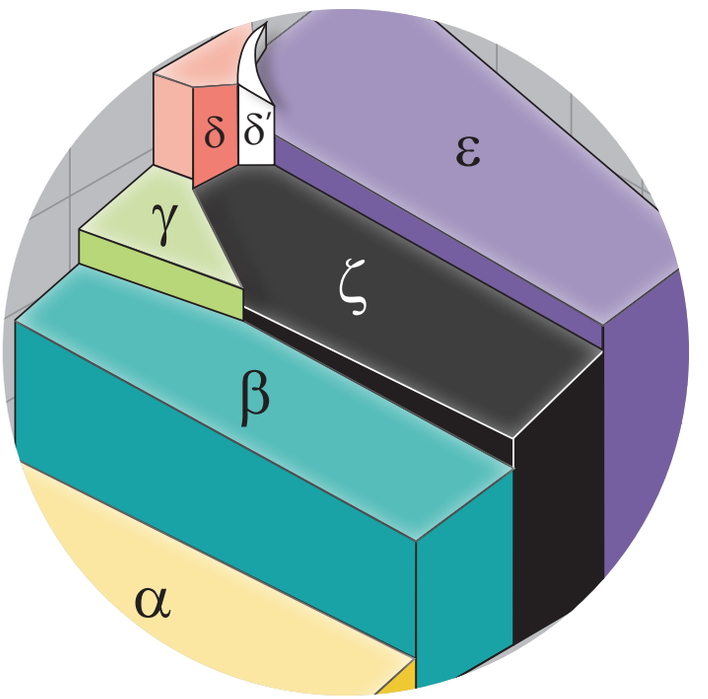

Ladislav Havela

Prof. Ladislav Havela from Charles University, Prague, presented his talk titled "Fingerprints of Electron Correlations in Various Phases of Plutonium: Electronic Properties of $Pu_{19}Os$ Simulating β-Pu" *at Pu Futures 2018 as a plenary speaker in Plenary Session VI.*

Fingerprints of Electron Correlations in Plutonium Phases: Electronic Properties of β-Pu Analogs

Ladislav Havela,[1] Silvie Maskova,[1] Pavel Javorsky,[1] Jindrich Kolorenc,[2] Eric Colineau,[3] Jean-Christophe Griveau,[3] Rachel Eloirdi,[3] Thomas Gouder[3]

The properties of plutonium are largely determined by electrons that occupy the open 5f electronic shell. These electrons are poised between localization and delocalization, and are difficult to describe using conventional theoretical frameworks which do not accurately account for pair correlations between electrons. Understanding such correlations and their impact on material properties is key to predicting the behavior of plutonium systems.

Metal properties in general depend on electrons in open shells—i.e., shells that are only partially filled. In most cases, they are outer s and p shells which strongly overlap between neighboring atoms in a crystal lattice, mediating the bonding between positive ions. Such electrons form a weakly-interacting fermionic liquid and occupy states with gradually increasing energy up to the so-called Fermi level, E_F. The basic properties of metals depend on how many states per atom are in close vicinity of the Fermi energy, because only those electrons can be thermally excited or redistributed by common external fields. Hence thermal, transport, and magnetic properties are critically dependent on this parameter, called density of states at the Fermi level, $N(E_F)$.

In some metals there are open shells of electrons that reside deep in the ionic core, with negligible overlap between neighboring ions. This is the case for the lanthanide 4f electrons. They do not contribute to bonding, but they can yield ionic magnetic moments, as spin and orbital moments within each 4f atomic shell are non-zero. Such localized electrons naturally do not contribute to $N(E_F)$.

The above two types of open shells are well understood by existing theories. In the case of the outer shells (i.e., delocalized electrons), conventional density functional theory (DFT) describes electron energetics as dependent on pair electron-electron (e-e) interactions in an implicit way, and the electronic states form bands of possible energies. For the inner shells (localized electrons), e-e correlations remain within the ion on which the particular electrons are localized. Electronic states remain discrete in the energy scale.

[1]*Charles University, Faculty of Mathematics and Physics, Ke Karlovu 3, CZ-12116 Prague 2, Czech Republic;* [2]*Institute of Physics, Czech Academy of Sciences, Na Slovance 2, CZ-182 21 Prague 8, Czech Republic;* [3]*European Commission, Joint Research Centre (JRC), Directorate for Nuclear Safety and Security, D-76125 Karlsruhe, Germany.*

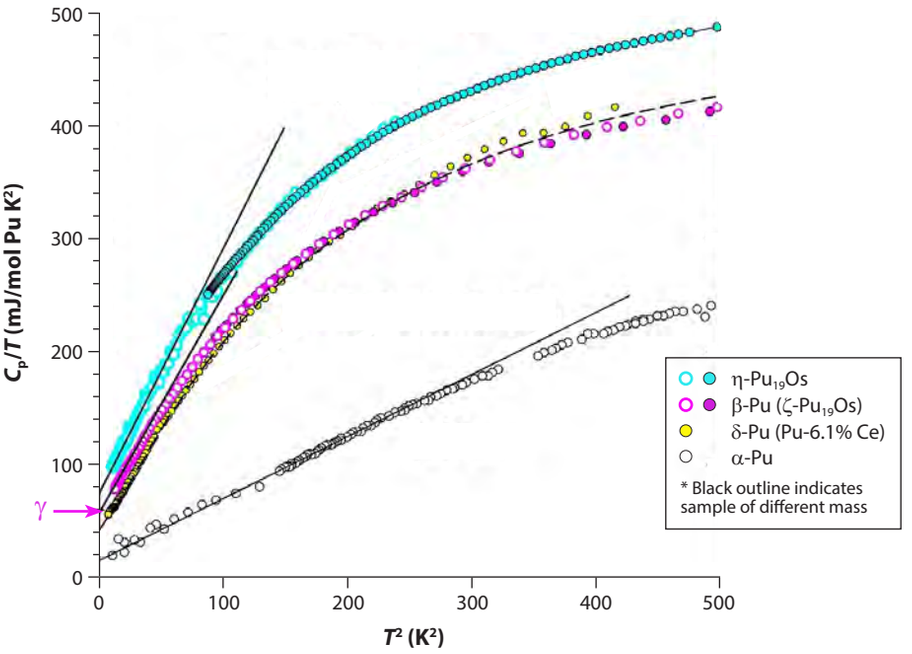

Figure 1. Temperature dependence of low-temperature heat capacity in the C_p/T vs. T^2 representation for ζ- and η-$Pu_{19}Os$ phases. The best low-temperature fits are shown, which give the Sommerfeld coefficient (γ) values as the vertical axis intercepts. The very high γ values for β-Pu (magenta arrow) and η-$Pu_{19}Os$ are unexpected and point to the importance of e-e correlations. The much steeper slopes of β- and δ-Pu compared with α-Pu indicate a softer crystal lattice (lower Debye temperature). [The β-Pu form is represented by the ζ-$Pu_{19}Os$ data, δ-Pu by Pu-6.1% Ce, and α-Pu from 2003 LANL data]

Neither of these two theoretical approaches are able to predict properties in cases with strong e-e correlations active in moderately localized states, which are intermediate between the two limiting situations discussed. Even worse, they cannot predict with sufficient precision if delocalization and bonding or localization and correlations within an atom (giving rise to the well-known Hund's rules) would give a lower total energy and thus be found experimentally. Although a more advanced paradigm of dynamical mean-field theory (DMFT) can successfully explain some thermodynamic or spectroscopic findings in select cases, actinides with 5f electronic states—which are generally more delocalized than lanthanide 4f states—still lack a general theoretical framework that can reliably identify different regimes and energy scales. This is particularly frustrating for studying elemental plutonium because it is on the verge of localization, which fully manifests for the next element in the period, americium.

An increase in volume per atom in a solid can reduce the bonding strength; therefore the existence of six plutonium allotropes with dramatically different atomic volumes suggests that the degree of 5f localization may be very different between them. But can these variations be simply understandable using the regular 5f bonding model that treats the 5f electrons as delocalized regardless of volume? It could be assumed, for instance, that the 5f states vary their nearest-neighbor overlap depending on a particular crystal structure modified for a given temperature range by the entropy of lattice vibrations. In this case, a lattice expansion would cause a higher $N(E_F)$ value as the electronic states have to be accommodated in a narrower energy band.

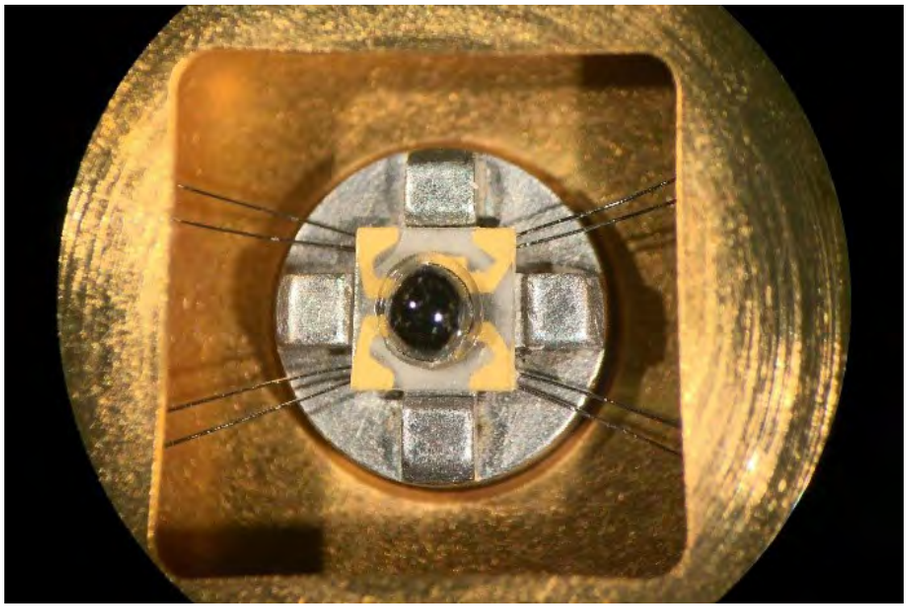

Figure 2. Sample mounting stage with a Stycast-coated transuranium sample (< 1 mm diameter) on a substrate with electrical contacts, heater, and thermometer. The necessary thermal contact is facilitated by a small amount of Apiezon grease under the sample. Inserted in a cryostat, the assembly is in a high-vacuum environment and suspended on thin wires, which also maintain a thermal contact.

Determination of density of states at the Fermi level, $N(E_F)$

To understand the behavior of 5f electrons it is important to determine $N(E_F)$ as a key parameter of the electronic system. Can this quantity be measured? The answer is yes and the way to do it is principally simple—by investigating the heat capacity at low temperatures.

The quantity that can be directly measured in a lab—the total heat capacity of a metal at a constant pressure, C_p—contains the electronic heat capacity and the heat capacity of lattice vibrations (phonons). The lattice contribution, which depends on the third power of temperature, can be subtracted by a simple trick, that is, plotting C_p/T versus T^2. The electronic contribution is characterized by the Sommerfeld coefficient γ, which can be obtained from this plot as the y axis intercept at linear extrapolation to $T = 0$ (Fig. 1). The Sommerfeld coefficient gives the density of states as γ is proportional to $N(E_F)$ in the simple band model (DFT). When the correlations are taken into account more accurately (Fermi liquid model), the situation is more complicated and this coefficient is given as $\gamma \sim N(E_F)/Z$, where $1/Z > 1$ and gets larger with increasing correlations ($Z = 1$ in DFT). The numerical factor Z can be approximated using theories going beyond DFT.

Accounting for self-heating effects

Measuring the total heat capacity is relatively straightforward—an isolated sample is subjected to a heat pulse and the resulting temperature increment is recorded. The necessary cooling to temperatures close to 0 K is a problem for plutonium however, due to radioactive decay-induced self-heating. A small piece of plutonium must be attached to a substrate (carrying a heater and a thermometer), the heat capacity of which is then subtracted. With a sub-milligram piece of plutonium one can reach temperatures below 5 K, but the accuracy of the specific heat determination is limited by the mass uncertainty. A reliable procedure relies on the measurement of several pieces with different mass, covering different temperature ranges. Radiological contamination was prevented in our procedures by coating the sample with a film of Stycast (an epoxy), the heat capacity of which must also be subtracted (see Fig. 2).

Density of electronic states

Electrons are fermions and each quantum state can therefore be occupied by at most one electron (Pauli exclusion principle). Gradually filling available states, the electrons occupy states with higher and higher energy. The highest energy reached, representing a boundary between occupied and empty states, is called the Fermi level, E_F. At normal temperatures, only electrons in close vicinity of the Fermi level can be excited to higher levels. The density of electronic states $N(E_F)$ is the number of states per an interval of energy in the close vicinity of the Fermi level.

The electronic component of the total heat capacity C of a metal is proportional to temperature T ($C = \gamma \cdot T$). The Sommerfeld coefficient γ directly reflects $N(E_F)$ together with a potential enhancement of the heat capacity due to correlations among electrons. Simple and noble metals have γ values around 1 mJ/mol K^2, values an order of magnitude higher are typical for transition metals, and the values of some of Pu phases reaching over 40 mJ/mol K^2 are the highest currently known among elements.

Heat capacity determination of phases unstable at low temperatures

The above method is clearly feasible for α-Pu, the monoclinic phase stable at low temperatures. But how to determine low-temperature C_p for other phases that exist only at high temperatures? By knowing that the δ-Pu fcc phase can be retained by alloying with a few percent of Al, Ga, or Am. This phase, used in applications due to its favorable mechanical properties, has an atomic volume 25% larger than α-Pu.

The difference in γ values between the α and δ phases is dramatic. Although γ = 17 mJ/mol K^2 for α-Pu, reported in 2003 by a Los Alamos National Laboratory (LANL) team, is comparable to α-U (10 mJ/mol K^2), the value for δ-Pu is much higher. The most recent analysis shows a value close to 40 mJ/mol K^2, which is more than double that for α-Pu. This exceptionally high value contrasts with figures for main-group and noble metals, which are only about 1 mJ/mol K^2.

Analysis of Sommerfield coefficient in α- and δ-Pu

What does this finding mean for the nature of the 5f states, in particular for their localization? α-Pu can be undoubtedly taken as a 5f band (delocalized) system. The γ-enhancement in δ-Pu can be due to either the narrowing of the 5f band caused by volume expansion (although calculations suggest that it would be difficult to avoid magnetic order in this scenario, and no such order is observed experimentally) or the increased importance of e-e correlations in the expanded lattice. These correlations are known to enhance the heat capacity since a thermal excitation of one electron induces excitations of other electrons. This many-body effect increases the thermal energy needed for a given temperature increment, therefore increasing the heat capacity. This mechanism of γ-enhancement is not as closely related to the volume and distance between neighboring atoms as the band mechanism.

Studies of β-Pu analogs

A key for distinguishing between different mechanisms leading to large γ values could be a low temperature study of other Pu allotropes. Unfortunately, none of these can be cooled far below room temperature using alloying, as was possible for δ-Pu. For β-Pu, a phase with a complex monoclinic structure and with volume intermediate between α- and δ-Pu, there is another possible approach. In 1979, the LANL crystallographer D. T. Cromer described a crystal structure of an intermetallic compound ζ-$Pu_{19}Os$. He noticed that the orthorhombic crystal structure has eight different Pu sites, seven of them being analogous to Pu sites in β-Pu. Its density is also practically

Table 1. Sommerfeld coefficient γ and Debye temperature Θ_D for Pu phases and $Pu_{19}Os$ alloys studied herein. Values of γ are given per mole of Pu for $Pu_{19}Os$ phases.

Phase	γ (mJ/mol K^2)	Θ_D (K)
α-Pu	17	153
β-Pu* (ζ-$Pu_{19}Os$)	55	101
η-$Pu_{19}Os$	74	96
δ-Pu (6.1% Ce)	41.5	103

* approximated by ζ-$Pu_{19}Os$

identical to that of β-Pu, corrected for thermal expansion, indicating similar distances between Pu neighbors. $Pu_{19}Os$ can thus serve as a β-Pu analog stable at low temperatures. Moreover, another structural variant with similar density, η-$Pu_{19}Os$, which is somewhat less similar to β-Pu, can be synthesized by annealing below 468 K. This provides an opportunity to explore low-temperature properties of both variants and compare them with existing data for α- and δ-Pu.

A low-temperature detail of the heat capacity in the C_p/T vs. T^2 representation (Fig. 1) illustrates the dramatic difference between α- and δ-Pu, the latter represented by an alloy with 6.1 at.% Ce. The derived Sommerfeld coefficients and Debye temperature data are listed in Table 1 (above), showing extremely high γ values for the β-Pu analogs.

Theoretical calculations

Conventional DFT, which assumes the validity of the band model of the electronic states, predicts a relatively low γ coefficient in both δ- and β-Pu phases, with values near 10 mJ/mol K^2. The underestimated value for δ-Pu is known to be a consequence of an oversimplified description of e-e correlations. Several groups have demonstrated that when these correlations are modeled more accurately using DMFT, the computed δ-phase γ coefficient becomes compatible with the experimentally measured value. Analogous correlated calculations have yet to be performed for β-Pu.

These calculations are very demanding because the β-Pu lattice has multiple crystallographic Pu sites, each experiencing a different environment. Nevertheless, they are not entirely impossible, as was recently demonstrated by a group of LANL and Rutgers University theorists, who successfully tackled the α-Pu phase that has a similarly complex crystal structure. In that study it was argued that although α-Pu behaves as an uncorrelated metal on average, some of the less-connected Pu sites in its lattice do exhibit signatures of strong correlations reminiscent of δ-Pu.

It is likely that the high γ values we observed for $Pu_{19}Os$ are a manifestation of strong e-e correlations near the less-connected Pu sites in the β-Pu-like lattice. To support this conjecture, we analyzed the behavior of the Sommerfeld coefficient γ under the assumption that all Pu sites are equivalent. In that case, the density of states at the Fermi level, $N(E_F)$, and with it the γ value, was found to monotonically decrease when the lattice volume is reduced, even if the e-e correlations are taken into account by means of DMFT (Fig. 3). The assumption of equivalent sites would therefore imply that the γ value for β-Pu lies between α- and δ-Pu values. This contradicts our experimental observations, however, and hence it must be the complexity of the β-Pu lattice in conjunction with e-e correlations that cause the observed γ enhancement.

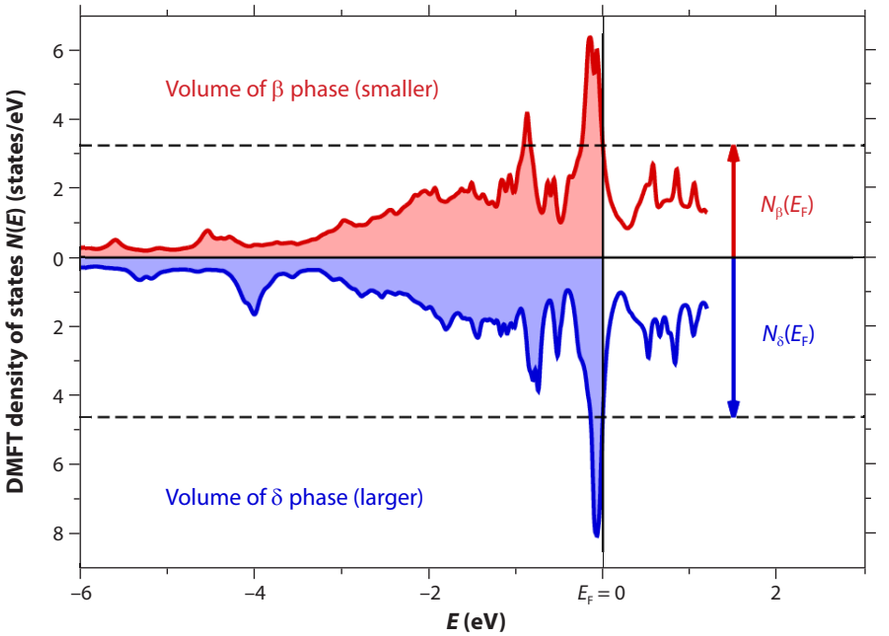

Figure 3. How would the Pu density of states change when the compression of the crystal lattice did not induce any structural change? I.e., if the crystal maintained the δ-Pu structure where all Pu sites are equivalent? DMFT calculations displayed above show that the density of states at the Fermi level, $N(E_F)$, would decrease with decreasing volume, $N_\delta(E_F) > N_\beta(E_F)$. The enhancement due to electron-electron correlations ($1/Z$) would display the same trend (not shown) and hence the Sommerfeld coefficient $\gamma \sim N(E_F)/Z$ would decrease with decreasing volume, which is opposite to the behavior found experimentally.

Summary

The β-Pu phase does not exist at low temperatures, where it transforms to the α phase, therefore its low-temperature heat capacity cannot be determined using direct methods. The β-Pu crystal structure is, however, very similar to that of $Pu_{19}Os$, which can be cooled close to the 0 K limit. This similarity allowed us to determine the Sommerfeld coefficient of the electronic specific heat for β-Pu. This quantity is of particular importance as it can be used to determine density of states, an essential parameter for predicting material properties. Its record-high value (55 mJ/mol K^2) exceeds values for both α- and δ-Pu, with smaller and larger volumes respectively. The non-monotonous behavior of the Sommerfeld coefficient as a function of volume cannot be explained by means of the conventional band theory, which implies that electron-electron correlations play a dominant role in β-Pu.

Further reading:

1. *The full story of the measurements of the heat capacity of $Pu_{19}Os$ and the discussion of their implications for the electron-electron correlations in β-Pu can be found in: L. Havela et al., Journal of Physics: Condensed Matter 30, 085601 (2018).*
2. *The structural similarity of ζ-$Pu_{19}Os$ and β-Pu is discussed by D. T. Cromer in Acta Crystallographica B35, 1945 (1979).*
3. *The computational demonstration of site-dependent correlations in α-Pu is reported in J.-X. Zhu et al., Nature Communications 4, 2644 (2013).*

Tonya Vitova

Dr. Vitova, a Scientist at the Institute for Nuclear Waste Disposal at Karlsruhe Institute of Technology, Germany, presented her invited plenary talk at Pu Futures 2018 during Plenary Session VIII. The talk was titled "Pu Electronic Structure and Speciation Applying Pu M_5 Edge HR-XANES and RIXS."

Paul Bagus

Dr. Bagus is a Research Professor at the University of North Texas. He was a keynote speaker at Pu Futures 2018 and gave his talk titled "Theoretical Analysis of the Properties of Pu(IV) and Pu (VI)" *in the Condensed Matter Physics I technical session.*

Probing Actinide Covalency: Plutonium Electronic Structure Studies Using High Energy Resolution X-Ray Spectroscopy

Tonya Vitova,[1] Horst Geckeis,[1] Paul S. Bagus[2]

The nature of chemical bonds in compounds with actinide (An) elements and the role of covalency is a topic of extensive research. Understanding these bonds ultimately allows us to design actinide material properties or predict their behavior in the environment. Covalency is a very important component of bonding that affects the chemical properties of a compound, and can be broadly defined for actinide complexes as the amount of mixing between metal-ligand orbitals in a bonding interaction. Advanced spectroscopic methods can provide new insights into the nature of these chemical bonds and can help the development and validation of theoretical approaches for predicting chemical and physical properties.

Principles of X-ray emission and absorption spectroscopy

One of the commonly used spectroscopic methods for studies of actinide materials is X-ray absorption spectroscopy (XAS). It is based on the absorption of X-ray radiation by atoms, leading to the excitation of a strongly-bound electron into an empty orbital that is only weakly bound. The resulting excited state decays or relaxes quickly through either the emission of electrons (photo- or Auger-emission) or X-ray fluorescence. The detection of these decay events is important to help us understand the nature of the An 5f and 6d shells, where the chemistry largely occurs.

XAS is element-sensitive because the characteristic electron binding energies are dependent on atomic number (Z); it is also angular momentum selective due to Fermi's golden rule. We can probe the amount of An f and d character of the unoccupied valence states by looking at different adsorption edges. Specifically, these include 3d→5f and 2p→6d excitations ($M_{4,5}$ and L_3 adsorption edges).

X-ray absorption spectra can be recorded in direct transmission geometry using the Lambert-Beer law to obtain the linear X-ray absorption coefficient while tuning the X-ray energy in the vicinity of an absorption threshold, i.e., the inner shell binding energy. The spectra can also be acquired by recording the intensity of a follow-up (relaxation) process—emission of electrons or characteristic X-ray fluorescence. Simplified schemes of the latter process for the M_5 absorption edge using the most intense characteristic fluorescence line M_α are shown in Fig. 2 (lines A and B). We focus herein on the first portion (< 200 eV) of the X-ray absorption spectrum, which is named X-ray absorption near edge structure (XANES; Fig. 1c,d).

[1]*Karlsruhe Institute of Technology (KIT), Institute for Nuclear Waste Disposal (INE), P.O. 3640, D-76021 Karlsruhe, Germany;* [2]*Department of Chemistry, University of North Texas, Denton, Texas 76203-5017, USA.*

(a) Solid-state detector used for XANES

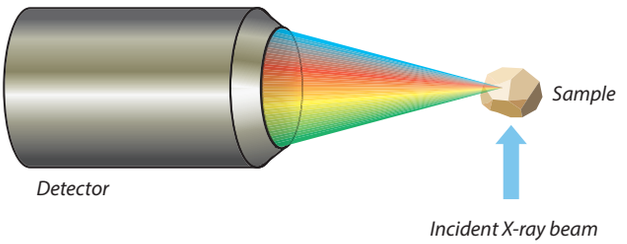

(b) Wavelength dispersive device used for HR-XANES

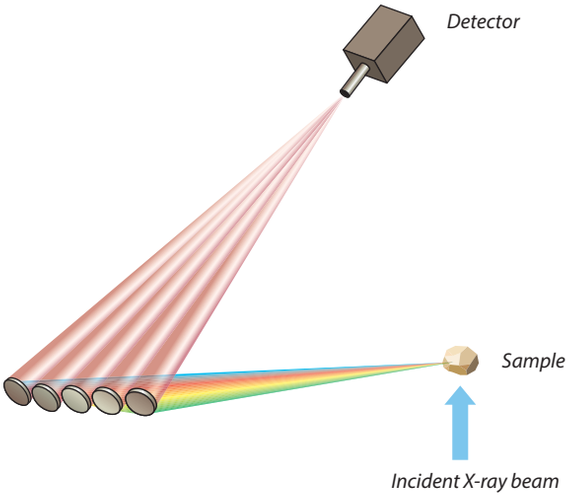

(c) Pu M_5 absorption edge

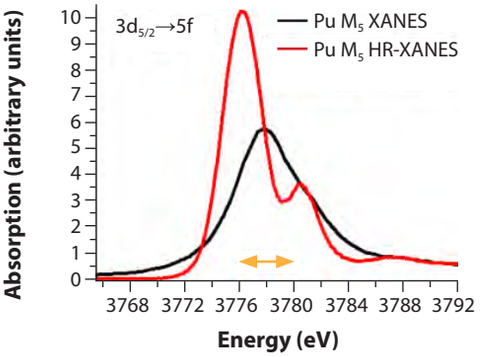

(d) Pu L_3 absorption edge

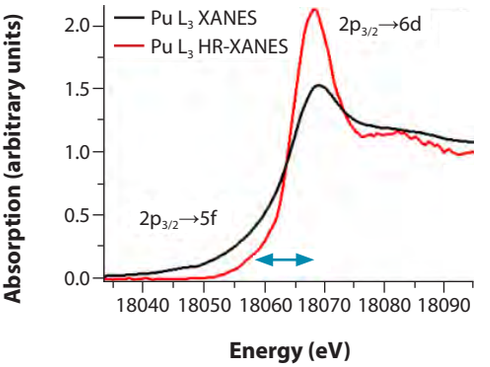

Limitations to spectroscopic resolution

The resolution of core-level spectroscopies such as XAS is limited by two factors: spectral broadening caused by the experimental setup and the lifetime of the ionized form of the atom (the core-hole state), which, from the quantum mechanical uncertainty principle, leads to an uncertainty in the energy of short-lived core-hole states.

The experimental energy resolution of XAS is tremendously improved if the emitted X-ray fluorescence (element-specific fluorescence line) is detected by a wavelength dispersive device following diffraction (i.e., analyzer crystals for hard to tender X-rays, 20–2 keV; Fig. 1b) instead of directly from a standard solid-state device with low energy resolution (such as a silicon-lithium or high-purity germanium detector; Fig. 1a). In this way, the L_3 and $M_{4,5}$ high-resolution XANES (HR-XANES) spectra are dramatically improved and exhibit a rich fine structure that cannot be resolved with conventional XAS detection setups (Fig. 1c,d). The lifetime of the core-hole in the final state is intrinsic and determines the spectral broadening.

An X-ray emission spectrometer also allows us to record resonant inelastic X-ray scattering (RIXS) maps. These maps depict a 2D representation of X-ray fluorescence emission measured as a function of excitation X-ray energy scanned across an absorption edge (Fig. 3, left). They allow us to detect energy shifts between emission lines measured at different excitation energies (see lines A and B in Fig. 2). It can be useful to compare HR-XANES spectra of different materials extracted from a RIXS map at specific emission energies.

Figure 1. Instrumental setups for (a) XANES and superior (b) high-resolution (HR) XANES. The latter employs a wavelength dispersive detector following diffraction rather than a standard solid-state device. The differences in the spectra obtained are shown in (c) Pu M_5 and (d) Pu L_3 absorption edge spectra—the black lines show data from the standard instrument, whereas the red lines give greater detail using the high resolution setup. The blue and orange arrows correspond to energy differences in Fig. 2. Spectra are for Pu(VI) in aqueous 1M perchloric acid ($HClO_4$) solution (PuO_2^{2+}).

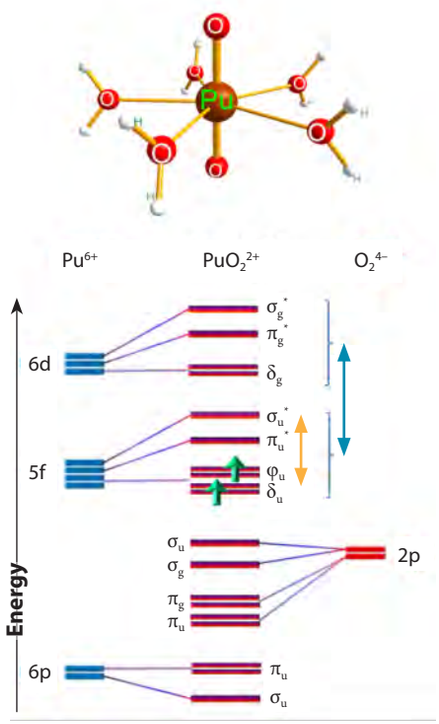

Figure 2. Schematic view (*top*) and molecular orbital scheme of plutonyl (*bottom*). The orange and blue arrows show the energy shifts between the different unoccupied orbitals measured in the spectra, as indicated in Fig. 1c,d.

Tools for studying covalency of the actinide chemical bond

The covalency of an actinide-ligand chemical bond can be significant when there is either a strong overlap or good energy match of metal and ligand valence orbitals. The concept of energy-degeneracy and orbital overlap driven covalency in actinide-ligand bonding was originally proposed by LANL teams in two articles titled "Determining relative f and d orbital contributions to M–Cl covalency..." and "Covalency in f-element complexes", published in the Journal of American Chemical Society (2012) and Coordination Chemistry Reviews (2013), respectively.

In order to explore chemical bond covalency in Pu complexes we studied a well-investigated material, Pu(VI) in aqueous 1M perchloric acid ($HClO_4$), using the M_5 edge HR-XANES and RIXS techniques. All experiments were performed at the INE-Beamline and ACT station of the CAT-ACT-Beamline at the Karlsruhe Research Accelerator (KARA) at the Karlsruhe Institute of Technology (KIT) in Germany.

Pu(VI) in $HClO_4$ forms strong, covalent trans-dioxo linear bonds (trans refers to the location of the oxygen atoms, on opposite sides of the metal ion; Fig. 2), termed plutonyl (PuO_2^{2+}) bonding. Five loosely-bound water molecules are also located in the equatorial plane of the plutonyl cation. A qualitative molecular orbital scheme of PuO_2^{2+} is depicted in Fig. 2; this also shows the orbital energy levels which are detected using the HR-XANES technique by observing the electronic transitions between the Pu 3d and 5f/6d orbitals. The linear structure of the PuO_2^{2+} ion means that the Pu valence orbitals are most usefully described in terms of their sigma, pi, delta, and phi character (with respect to rotation about the axial Pu–O_{ax} z-axis).

Overlap-driven covalency

The seven empty or partially-occupied 5f orbitals of the PuO_2^{2+} cation (Fig. 2) are split by the ligand field of the axial and equatorial ligands, and spin-orbit coupling. When there is more than one electron in the 5f shell, Coulomb repulsions between the electrons become important. The spin-orbit splitting of the 5f electrons is approximately 1 eV while the ligand-field splitting can be as large as 7 eV for actinyl species. Matsika described in "Electronic structure and spectra of actinyl ions", published in the Journal of Physical Chemistry A in 2001, that the influence of these effects can be ordered as follows: axial ligand field effects on 5f-based sigma and pi anti-bonding orbitals > Coulomb repulsion > spin-orbit coupling > summed effects of axial and equatorial ligand fields on the 5f-based delta and phi orbitals.

The axial field exerts the greatest effect, caused by the strongly covalent nature of the An–O_{ax} (An = U, Np, or Pu) bond manifested by the large overlap of the An (5f, 6p) and O (2p) orbitals. As a result, the 5f sigma and pi anti-bonding orbitals are shifted with respect to the 5f delta and phi orbitals (delta ≈ phi < pi anti-bonding << sigma anti-bonding; Fig. 4); this effect is called "pushing from below". Pu $M_{4,5}$ absorption edge HR-XANES and RIXS spectra display electronic transitions of 3d electrons to 5f delta/phi and pi/sigma anti-bonding orbitals in the same spectrum (Figs. 1c, 3, and 4).

Due to the improved instrumental resolution it was possible to measure energy differences between the 5f delta/phi and the 5f pi/sigma anti-bonding peaks. We propose using changes in these energy shifts, specifically between the 5f delta/phi and the 5f sigma anti-bonding peaks, as a qualitative measure of changes in the overlap-driven covalency of the actinyl bond. We found that these energy differences decrease in the order UO_2^{2+} > NpO_2^{2+} > PuO_2^{2+} (Fig. 4), suggesting that the overlap-driven covalency of the An–O_{ax} bond decreases similarly. This is consistent with the intuitive view that the 5f orbital size decreases as the nuclear charge increases from U to Pu.

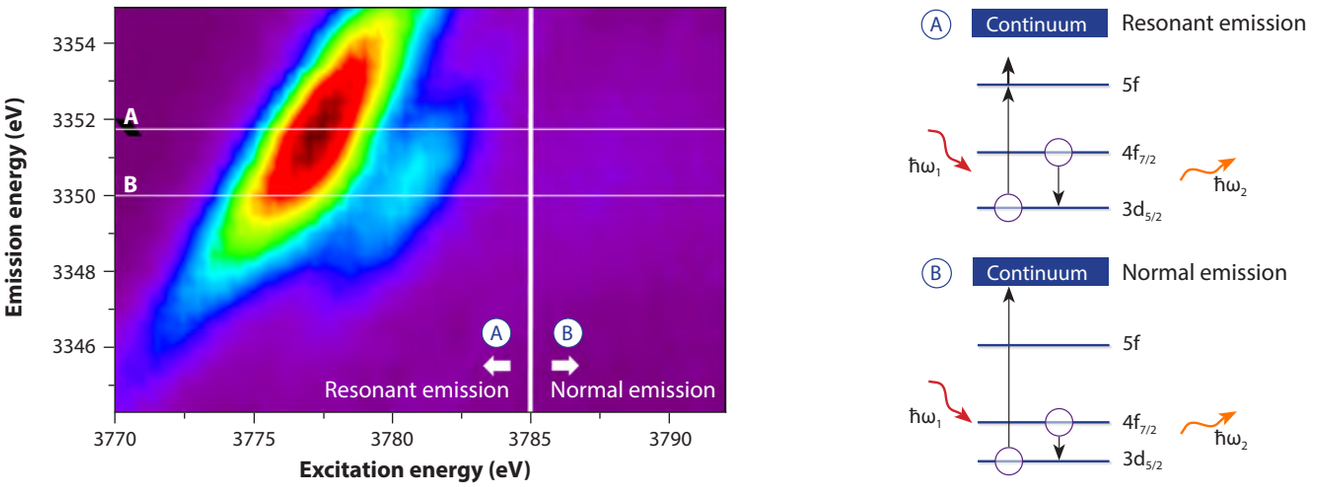

Figure 3. Resonant inelastic X-ray scattering (RIXS) map, *left*, depicts characteristic Pu M_α fluorescence at the Pu M_5 absorption edge. Horizontal lines A and B show maximum intensities of the most intense resonance and normal emissions; the shift between these lines reflects the gaps between the $4f_{7/2}$ and $3d_{5/2}$ states (*right*). Schemes A and B show resonant and normal emission, respectively, when the electron is excited into either unoccupied 5f orbitals or the continuum (i.e., the atom is ionized); circles represent core holes.

Energy degeneracy-driven covalency

Changes in energy degeneracy-driven covalency can be estimated by comparing the degree of An 5f orbital localization within a series of materials using RIXS maps. The PuO_2^{2+} map and a simplified one-electron scheme describing the emission process are shown in Fig. 3. The 3d electrons are predominantly excited to unoccupied states with substantial 5f character. The RIXS map can be divided into resonant and non-resonant (normal) emission (vertical line in Fig. 3); these describe processes in which the electron is excited to bound unoccupied states and to the continuum, respectively, both with subsequent 4f→3d Pu M_α emission (Fig. 3 A,B).

This shift in emission energy of the resonant peaks with respect to normal emission (shift between horizontal lines A and B in Fig. 3) accounts for the strong interaction between the excited electron in the lowest unoccupied bound electronic states and the created core-hole, which differs from the ionized case. The energy shift between lines A and B therefore probes the localization of those lowest unoccupied 5f states on the absorbing atom; this effect is described schematically in Fig. 3. We found an increase in energy shift going from U to Pu in the actinyl system suggesting that the 5f orbitals undergo stronger localization in the order $UO_2^{2+} < NpO_2^{2+} < PuO_2^{2+}$.

The effect of multiplet splitting and ligand field on plutonyl spectrum

An important contribution to the width of the observed XANES peaks is from coupling between the open shell electrons which show multiplet signals with slightly different energies. These multiplets arise from angular momentum coupling of the open shell electrons, both for the core hole as well as the open 5f shell. Because the small energy differences cannot be resolved experimentally, theoretical calculations can help us understand their presence and how they shape the observed spectra.

Multiplet calculations were implemented for excitations in both an isolated Pu^{6+} ion and for the plutonyl ion (Fig. 5, blue and green lines). The first approach did not allow for covalent bonding, but allowed us to study the effect of "ideal" multiplets. The second accounted for both angular momentum coupling and covalent bonding.

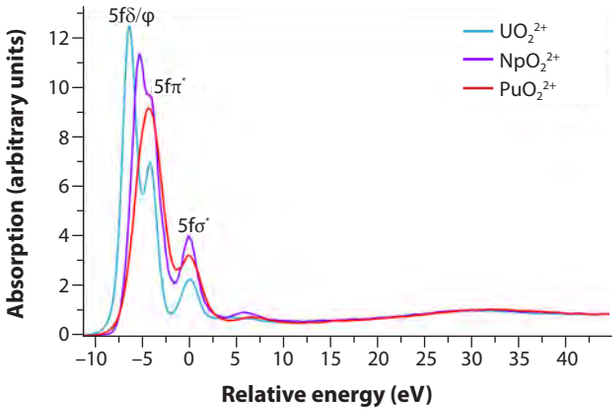

Figure 4. $M_{4/5}$ absorption edge HR-XANES spectra showing electronic transitions from An 3d- to 5f-based molecular orbitals. The energy shift between the first peak and the subsequent ones decreases from U to Pu, which can be interpreted as decreasing overlap-driven covalency of the actinide-ligand bond. Due to the increasing number of valence electrons the intensity of the first peak significantly decreases going from U (f^0) to Pu (f^2).

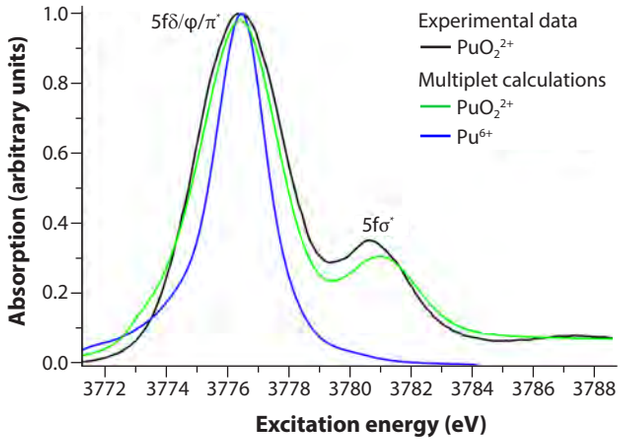

Figure 5. Pu M_5 absorption edge HR-XANES experimental (black) and calculated (green) spectra of PuO_2^{2+} and a calculated spectrum of Pu^{6+} (blue). We can see a better fit with the calculations in which the Pu–O interaction is explicitly taken into account, as opposed to the more simplistic isolated Pu^{6+} ion. The spectral peak labels correspond to orbitals in Fig. 2.

Acknowledgments

This work is a joint effort from many scientists primarily at the Institute for Nuclear Waste Disposal (INE), Karlsruhe Institute of Technology (KIT), Germany who are authors of the first two publications listed in Further Reading. We acknowledge the Helmholtz Association of German Research Centers for the VH-NG-734 grant and the Karlsruhe Research Accelerator (KARA) for provision of beam time. PSB acknowledges support from the U.S. Department of Energy, Office of Science, Office of Basic Energy Sciences, Chemical Sciences, Geosciences, and Biosciences (CSGB) Division through the Geosciences program at Pacific Northwest National Laboratory.

The spectrum calculated for Pu^{6+} without any considerations of covalent mixing shows a broad main peak, without the higher energy peak at 3781 eV. The multiplet plutonyl model meanwhile, in which the covalent mixing is taken into account, shows agreement between theory and experiment, and clearly shows that the ligand field is important for a correct theoretical description of the PuO_2^{2+} spectrum.

Summary

We have illustrated that HR-XANES and RIXS are very useful tools for characterizing actinide electronic structures and can be applied to any type of materials, under static or dynamic conditions—for example at elevated temperatures, high pressures, or during chemical reactions. RIXS allows direct comparison of the amount of 5f orbital localization. Changes in the relative energy differences between the AnO_2^{2+} 5f delta/phi and the 5f pi/sigma anti-bonding orbitals, determined from the An $M_{4,5}$ edge HR-XANES spectra, provide a qualitative measure for the level of overlap-driven covalency in the actinyl bond. The observed trends in these energy differences indicate that U(VI)–O_{ax} is more covalent compared to the Np(VI)–O_{ax} and Pu(VI)–O_{ax} bonds. We have shown that electron-electron interactions lead to broadening but are not the dominant effect in the An $M_{4,5}$ absorption edge HR-XANES spectra of the actinyl species. The axial ligand field plays the most important role and therefore needs to be considered in calculations.

Further Reading:

1. *T. Vitova et al. "The role of the 5f valence orbitals of early actinides in chemical bonding"; Nature Communications, 2017, 8, 16053.*
2. *T. Vitova et al. "Exploring the electronic structure and speciation of aqueous and colloidal Pu with high energy resolution XANES and computations"; Chem. Commun. 2018, 54, 12824.*
3. *P.S. Bagus et al. "Covalent Bonding In Heavy Metal Oxides"; J. Chem. Phys. 2017, 146, 134706.*
4. *S.G. Minasian et al. "Determining Relative f and d Orbital Contributions to M–Cl Covalency in MCl_6^{2-} (M = Ti, Zr, Hf, U) and $UOCl_5^-$ Using Cl K-Edge X-ray Absorption Spectroscopy and Time-Dependent Density Functional Theory", J. Am. Chem. Soc. 2012, 134, 5586.*
5. *M.L. Neidig et al. "Covalency in f-element complexes", Coord. Chem. Rev. 2013, 257, 394.*

Plutonium Metal Corrosion by Water Vapor: An X-Ray Photoelectron Study

Lionel Jolly, Pascal Berthou, Brice Ravat, Benoît Oudot, François Delaunay
CEA Valduc, F-21120 Is-sur-Tille, France

Plutonium metal is particularly susceptible to corrosion, even under ambient conditions. Although this corrosion is controlled industrially, the details of the mechanisms are not well understood and remain controversial, especially in the presence of H_2O. The purpose of this study is to describe the first stages of plutonium metal corrosion mechanisms under water vapor exposure. Understanding these initial stages is important because they drive the corrosion process. X-ray photoelectron spectroscopy (XPS) is useful for studying various properties of surfaces, e.g., composition, chemical and electronic properties, and oxidation state. This technique provides an image of the electronic structure of the surface where corrosion reactions take place.

Plutonium metal has a high chemical reactivity. Two types of oxide form under an oxidizing atmosphere—an inner sesquioxide, Pu_2O_3, in contact with the metal and an outer dioxide layer, PuO_2, in contact with the gas. The thickness and the ratio between both oxides depend greatly on the exposure conditions (e.g., temperature, gas pressure, exposure time). Corrosion kinetics experiments (e.g., monitoring weight gain) show that plutonium metal forms a protective oxide layer under oxidant gas. Under certain conditions, this layer can be damaged, sharply enhancing the oxidation rate. Thus, even at room temperature, corrosion may be severe for long-term storage in an atmosphere that is not well controlled.

X-ray photoelectron spectroscopy and Tougaard analysis

XPS is a technique based on the photoelectric effect that provides information about the nature and valence of atoms related to their chemical environment. Typically, this information is obtained from the chemical shift of the binding energy of elastic photoelectrons, corresponding to the observed peaks in the XPS spectra (Fig. 1).

A new method has been recently developed by S. Tougaard (University of South Denmark) which allows surface nanostructure information can be extracted from the background portion of XPS spectra. The transport of photoelectrons in matter depends on the nature of the material, surface geometry, and kinetic energy, which is lost as photoelectrons pass through the solid. Thus, the shape and intensity of the background of the spectra are indicative of surface nanostructure (Fig. 2).

Experimental considerations

This study consisted of applying low exposures of water vapor to a plutonium metal surface. An initial surface was prepared before each exposure—the challenge was to prepare "perfect" plutonium metal without traces of oxide or carbon contamination ("adventitious" carbon). These traces are due to the extreme reactivity of the metal—plutonium is so reactive that we can expect that the oxidant gas is in contact with an oxide, never with the metal. Therefore, the choice was made to prepare a slightly oxidized metal surface for this first approach which was as clean as possible.

Lionel Jolly

Dr. Jolly is a Scientist at the French Alternative Energies and Atomic Energy Commission (CEA) Centre de Valduc. He presented his talk titled "Photoelectron Spectroscopy Study of H_2O Adsorption and Dissociation on Oxidized Pu Metal" *in the Surface Science and Corrosion II session at Pu Futures 2018.*

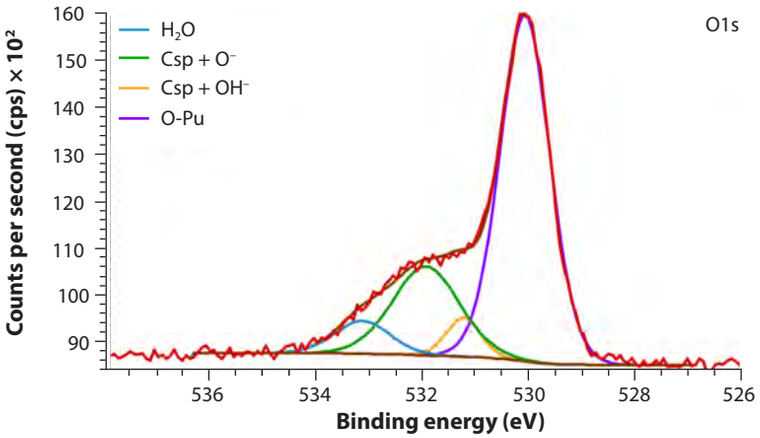

Figure 1. Components of the oxygen 1s core level photoemission peak after 1 mbar exposure of water vapor on Pu metal for five minutes. This peak is comprised of four components with shifts in binding energy due to the different chemical environments of the oxygen atoms. The main component is linked to the O^{2-} in the bulk of both oxides. The three secondary components are OH^- hydroxyl groups, O^- subsurface defects, and H_2O quasi-chemisorbed molecules. A portion of these secondary components is linked to carbon species (Csp) that come from adventitious carbon.

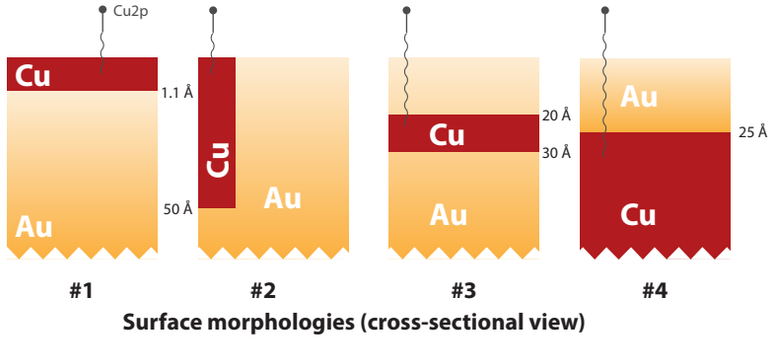

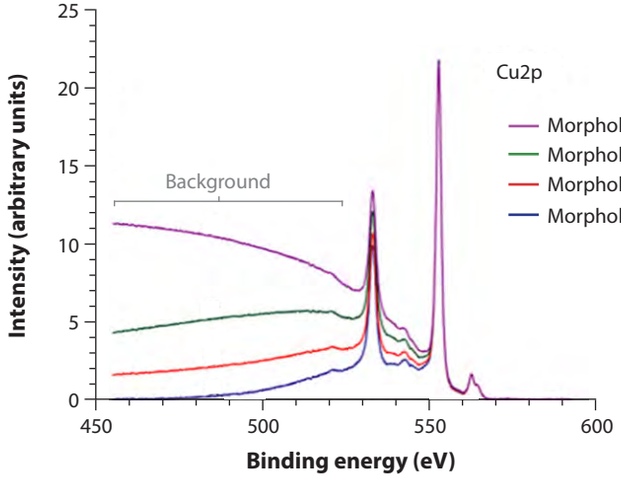

Figure 2. This example from the literature shows how inelastic photoelectrons produce a background in the spectra (*below*). This example for the background of a copper 2p core level photoemission peak in a gold matrix shows how the intensity and the shape of the background, as different surface morphologies #1–4 carry surface nanostructure information (figure adapted from Tougaard, 2010). Therefore the background portion of the spectrum can provide information about the surface.

The plutonium sample surface was prepared by electropolishing followed by several cycles of Ar^+ sputtering and heat treatments. This procedure made it possible to obtain identical surfaces before each exposure, which were considered to be sufficiently clean (< 3 at.% carbon a few nanometers deep), and composed mainly of Pu_2O_3 with a small amount of PuO_2 and metal. These samples were exposed to a water vapor pressure ranging from 5×10^{-7} to 1 mbar at room temperature for five minutes. The short duration of exposure allowed gas and surface radiolysis phenomena to be neglected.

Spectroscopic results

We can deduce that only Pu^{III} (Pu_2O_3) and Pu^{IV} (PuO_2) are present on the surface from the analysis of the photoemission peak of the Pu 4f peak. The O 1s peak

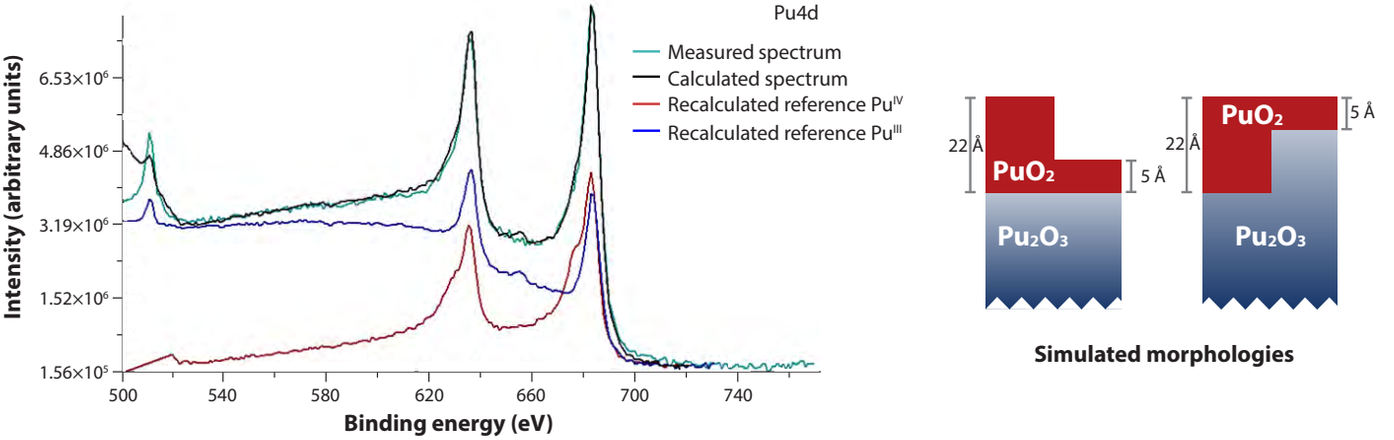

Figure 3. Tougaard analysis of the background of the plutonium 4f core level photoemission peak after 10^{-6} mbar water vapor exposure for five minutes. Reference spectra are calculated as a function of the surface morphologies, *right*. The red cross-sections represent new PuO_2 growth, the blue is the native Pu_2O_3 layer. In this particular case, both simulated morphologies give the same result in term of spectra, therefore the formed PuO_2 islands can grow in or out of the native layer.

meanwhile is formed of several different components—several chemical species are found which vary in concentration or appear during exposure (Fig. 1). In spite of the contribution of carbon species to the O 1s peak, four different species were identified with the help of a comprehensive study on oxides performed by Dupin and co-workers at the Centre National de la Recherche Scientifique, Hélioparc Pau-Pyrénées, published in the article "Systematic XPS studies of metal oxides, hydroxides and peroxides," in Physical Chemistry Chemical Physics in 2000.

The main component is correlated with O^{2-}, the type of oxygen ion associated with bulk oxides. Three secondary components can also be distinguished which include carbon species from traces of adventitious carbon. After fitting and comparison of spectra before and after exposures, the variations of these three components show that they are mainly connected to hydroxyl groups (OH^-), subsurface defects, and so-called "quasi-chemical" H_2O molecules (Fig. 1). The subsurface defects are considered oxygen ions with lower electron density than O^{2-}, i.e., O^- type. The H_2O molecules are described as "quasi-chemical" because they are attached to the surface hydroxyl groups by hydrogen bonding, as described Stakebake at DOW Chemical USA in the article "A thermal desorption study of the surface interactions between water and plutonium dioxide", in the Journal of Physical Chemistry, 1973. Tougaard analysis of the spectra describes the morphology of PuO_2 oxide growth at the surface (Fig. 3).

Plutonium oxidation mechanism under water vapor

A novel description of metallic plutonium oxidation mechanisms under water vapor can be developed by combining these results with the literature. XPS data show that, despite a major contribution of Pu^{III} to the intensity of the Pu 4f peak, the initial surface is covered by a relatively thin layer (~5 Å) of Pu^{IV} in the form of PuO_2 (Fig. 4-1). As soon as the surface is exposed to water vapor, H_2O molecules dissociate into hydroxyl and hydrogen ions. The hydrogen ion is bound to an oxygen atom of the native PuO_2 layer. As previously observed with the effect of water vapor on UO_2, the hydroxyl oxygen atoms diffuse into the oxide via surface defects to form new PuO_2. Thus, PuO_2 islands form in the vicinity of the PuO_2 native layer (Fig. 4-2).

Tougaard analysis suggests that these PuO_2 islands are ~2 nm thick and first grow laterally but it does not allow us to determinate if these islands grow in or out of the native layer (Fig. 3). Both cases are possible and depend on the type of diffusion during oxidation. Inner oxide growth means that oxidation is driven by anionic diffusion (preferential diffusion of oxide anions towards the oxide/metal interface); reciprocally, outer growth is driven by cationic diffusion (metal cation diffusion to interface).

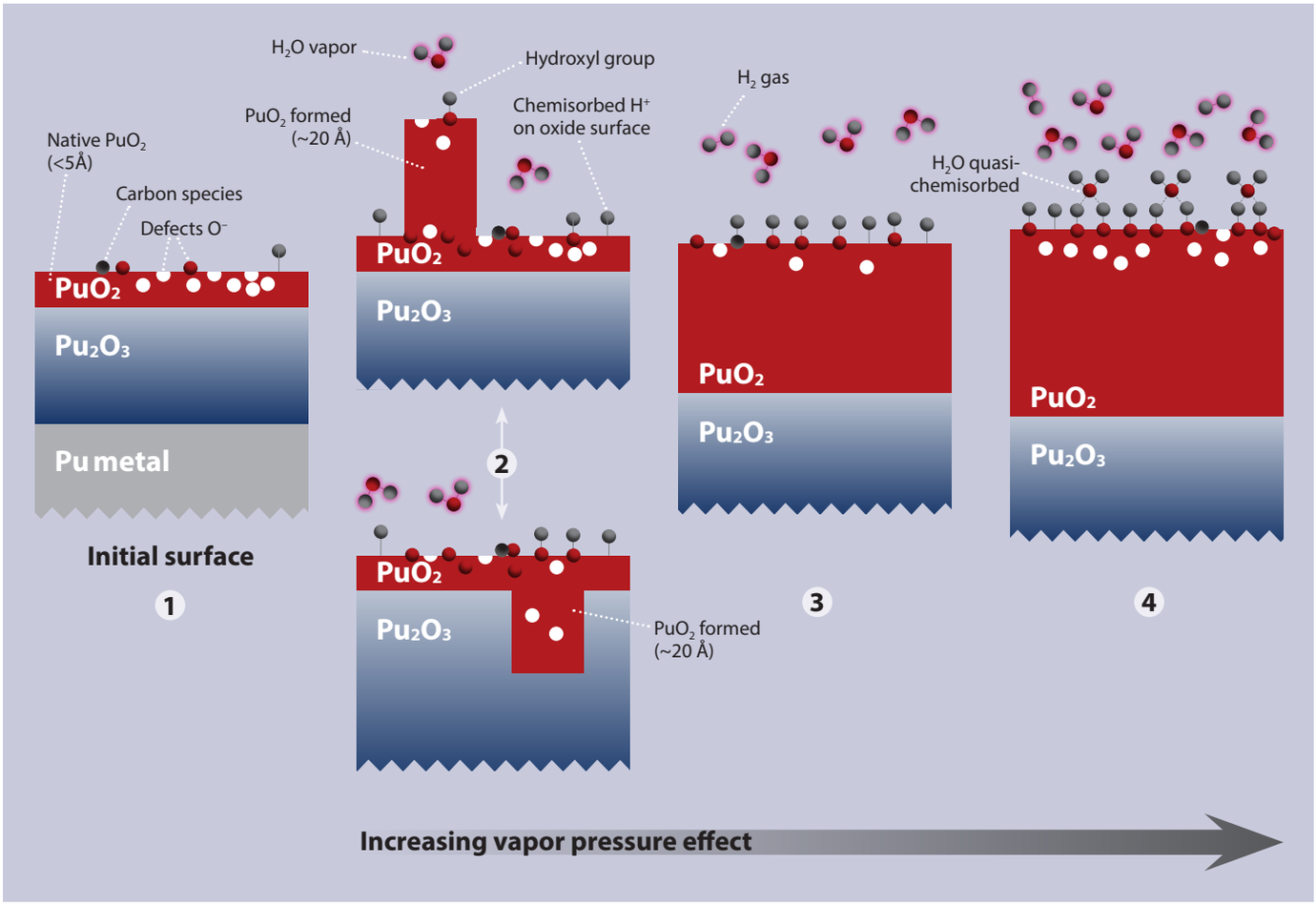

Figure 4. Schematic representation of the novel corrosion mechanisms described for plutonium metal (coated with a thin oxide layer as found experimentally) with water vapor at room temperature.

At a water vapor pressure higher than 10^{-4} mbar after five minutes exposure, the islands form a PuO_2 layer with a homogeneous thickness. Its thickness then gradually increases as a function of exposure. Hydrogen ions, which result from H_2O dissociation, bond and desorb as H_2 gas. However, hydrogen ions may be introduced into the oxide through subsurface defects, as already observed for other metal oxides such as NiO (Fig. 4-3). This work shows that H_2O molecules "quasi-chemisorb" (i.e., bond via hydrogen bonds) onto hydroxyl ions after reaching a certain coverage rate (Fig. 4-4), while the continuous PuO_2 layer thickens gradually.

Summary

Understanding the corrosion mechanisms of plutonium is important to control the properties and degradation of this reactive metal more precisely. Our XPS investigation has allowed us to describe the first steps of corrosion using an innovative simulation of the background of photoelectron spectra. We have gained insight into the interaction and dissociation of H_2O molecules on a slightly oxidized Pu metal surface and subsequent PuO_2 formation, which initiates at a thickness of approximately 2 nm. Investigations continue to determine the diffusion in the oxidation process and the oxide growth kinetics at both nano- and microscopic scales.

Further Reading:

1. *S. Tougaard, "Energy loss in XPS: Fundamental processes and applications for quantification, non-destructive depth profiling and 3D imaging", 2010, J. Electron Spectros. Relat. Phenomena, 178–179, 128.*

Modeling the High Temperature Phase of Plutonium

Boris Dorado, François Bottin, Johann Bouchet
CEA, Centre DAM Ile de France, 91297 Arpajon, France

Plutonium is an actinide whose radiotoxicity makes high temperature experiments difficult to perform. Therefore, atomic scale modeling is a relevant tool to investigate temperature-dependent phenomena, in particular the details of the plutonium phase diagram. The full ab initio calculation of this diagram remains challenging, however. Plutonium crystallizes into six different allotropic forms at ambient pressure (Fig. 1). Each of these phases provides challenges for ab initio methods, the delta phase in particular epitomizing these difficulties. Indeed, one of the main obstacles presented by delta-plutonium stems from the occurrence of valence fluctuations—electrons around the nucleus constantly move from one orbital to the other, resulting in dynamical orbital mixing that theories have long failed to describe. It is only with the advent of appropriate theories, such as the dynamical mean field theory, that these valence fluctuations can be accounted for. As a consequence, it has taken more than 40 years of combined experimental and theoretical work to unveil the electronic mechanisms that govern this phase of plutonium. The epsilon phase—the crystalline structure adopted above 730 K—is even less well understood, with very little experimental or theoretical data available, owing to safety issues with radiotoxicity and handling.

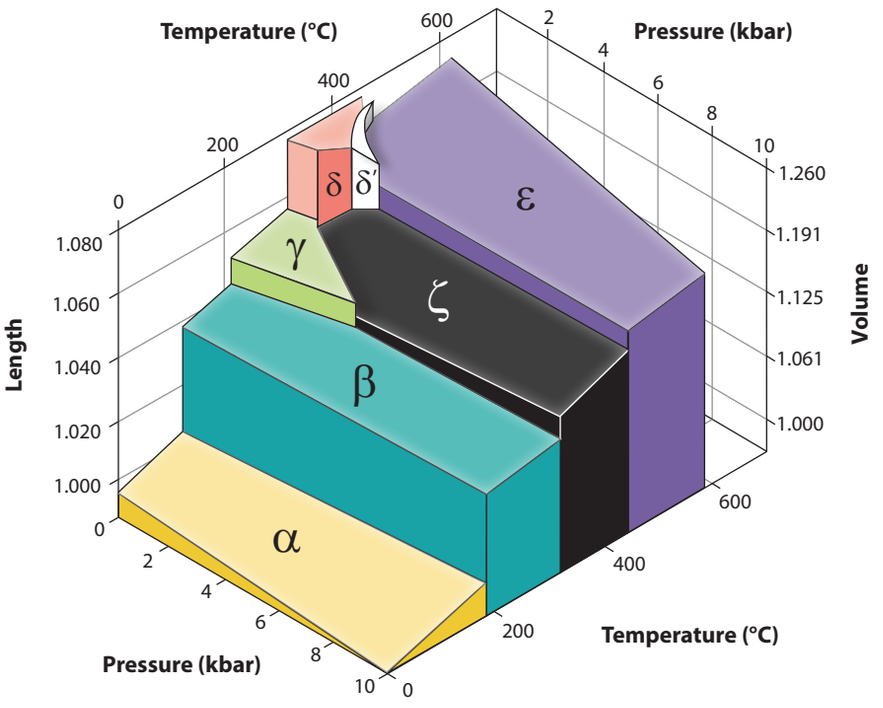

Figure 1. Plutonium phase diagram (adapted from J.R. Morgan, Los Alamos National Laboratory 1970).

Boris Dorado

Dr. Dorado is a Research Scientist at the French Alternative Energies and Atomic Energy Commission (CEA) Centre DAM Ile de France. He presented his talk "Unifying DFT+U Approach for Plutonium Modeling" during the Condensed Matter Physics II technical session at Pu Futures 2018.

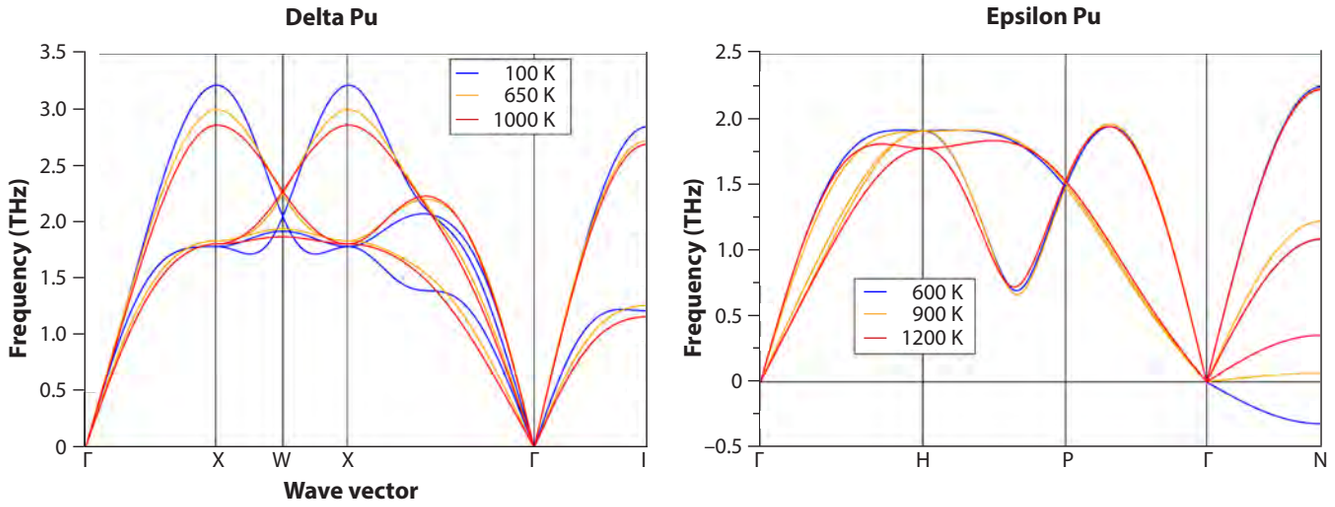

Figure 2. Simulated phonon spectra of the delta and epsilon phases of plutonium, left and right respectively, calculated at different temperatures between 100 and 1200 K. The letters on the horizontal axis represent specific points in space. The Γ point, for instance, is located at the center of the crystal, while the other points have more complex locations within the crystal but are generally points with a high number of crystal symmetries. The delta phase shows similar spectra regardless of temperature (100–1000 K), indicating dynamical stability, however the epsilon phase only shows this stability at higher temperatures (above 600 K).

Although the key parameter for the plutonium phase diagram is temperature, all previous ab initio studies have been carried out at zero kelvin, mainly due to computational limitations. In order to include temperature effects, the vibrational properties of the material have to be calculated; that is, the spatial dependence of the vibrational frequencies of plutonium atoms. Analysis of these frequencies gives several thermodynamic quantities that are required for modeling the phase diagram.

Approach

In order to calculate the vibrational frequencies, we used the electronic structure code ABINIT, co-developed at CEA (French Commission for Atomic and Alternative Energies), on the Tera-1000 supercomputer—the most powerful European general-purpose supercomputer currently in use, with a computing power of 25 petaflops (Fig. 3). In these calculations, the two most important physical effects have been accounted for: (i) temperature, using the TDEP method (temperature-dependent effective potential) and (ii) localization of the plutonium electrons, hence the "correlated" denotation, with a formalism that uses density functional theory (DFT) together with a Hubbard correction for correlations. In the TDEP method, frequencies are calculated by diagonalizing the dynamical matrix, which links the forces and atomic positions obtained through the molecular dynamics simulation.

Simulated phonon spectra

The phonon spectra (Fig. 2) of both the delta phase, which is dynamically (i.e., mechanically) stable between 580 and 730 K, and the epsilon phase, which is likewise stable between 730 and 900 K (a phonon is a discrete unit, or quantum, of vibrational mechanical energy, in the same way as a photon is a quantum of electromagnetic energy). The spectra have been calculated at three different temperatures. For a given phase and temperature, the curves depict the vibrational modes of the crystal at different points in space—as with sound and light waves, the crystal vibrations are a superposition of waves with different spatial frequencies (or wavelengths) in different directions, as indicated by wave vectors and letters indicating points of lattice symmetry. Furthermore, several calculations have been performed at temperatures that are outside the range of the phase stability in order to better understand how phonon spectra evolve with respect to temperature.

Figure 3. The Tera-1000 supercomputer. With 25 petaflops computing power it is the most powerful European general-purpose supercomputer in use. It was developed in 2018 at the CEA (French Alternative Energies and Atomic Energy Commission) center in Bruyères-le-Châtel (Île-de-France).

We found that the phonon spectrum of the delta phase is not significantly affected by temperature effects. The crystal is then referred to as "harmonic", up to 1000 K. We also observed that all the frequencies in the delta phase phonon spectrum are positive, which indicates that the crystal is dynamically stable. The phonon spectrum of the epsilon phase has not been previously obtained, meanwhile, either experimentally or theoretically. We observed that some frequencies are negative in the Γ-N direction, which indicates that the phase is not dynamically stable at this temperature (600 K); however, the phase gradually stabilizes with increasing temperature.

Summary

Ab initio molecular dynamics simulations have been performed in order to study the dynamical stability of the high temperature phases of plutonium (delta and epsilon). Several calculations have been carried out simulating temperatures between 300 and 1200 K, and the vibrational frequencies of plutonium atoms have been subsequently analyzed in both crystalline phases. We have shown that the epsilon phase can be stabilized at high temperature, provided that both electron correlation and temperature effects are simultaneously accounted for. Calculations also show that, in contrast to the delta phase, vibrational frequencies in the epsilon phase vary significantly with respect to temperature.

Further reading:

1. *J. R. Morgan in Plutonium (1970) and Other Actinides: Proc. 4th Int. Conf. on Plutonium and Other Actinides; Miner, W. N., Ed.; Metallurgical Society of the American Institute of Mining, Metallurgical, and Petroleum Engineers: Santa Fe, New Mexico, (1970), p669.*


ANS Meetings
Plutonium Futures–
The Science 2018
A Topical Conference on
Plutonium and Actinides
Thank You to our
2018 Co-Sponsors!
Los Alamos
NATIONAL LABORATORY
EST. 1943
Lawrence Livermore
National Laboratory


American Nuclear Society
Actinide Research
Quarterly
Los Alamos National
Laboratory
ANS
Plutonium Futures—
The Science 2018
A Topical Conference on Plutonium and Actinides


ANS Plutonium Futures–
The Science 2018
Welcome to Plutonium
Futures–The Science 2018

Plutonium Futures
The Science 2018

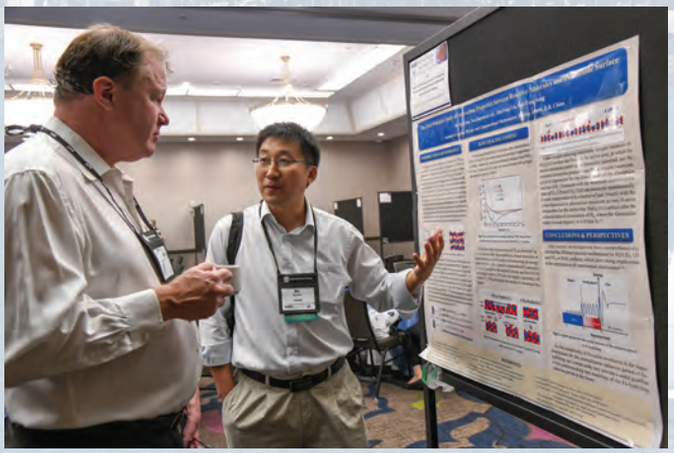

Best Student Posters Plutonium Futures 2018

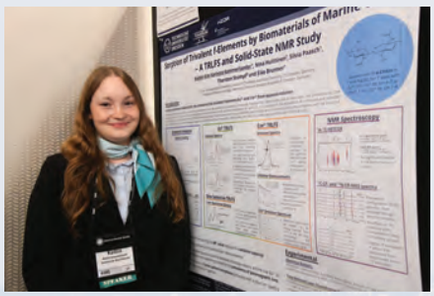

PLUTONIUM FUTURES

Sorption of trivalent f-elements by biomaterials of marine origin—a TRLFS and solid-state NMR study

Kaitlin Kim Karlotta Kammerlander
Technische Universitaet Dresden, Germany

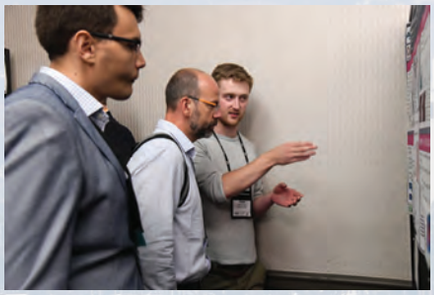

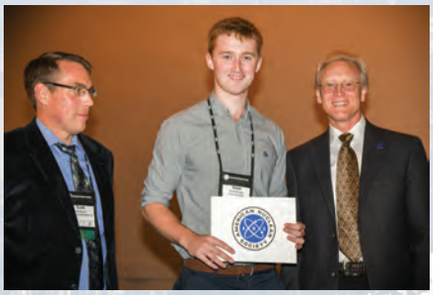

METALLURGY & MATERIALS SCIENCE

Trivalent impurities promote oxygen vacancy segregation and increase oxygen transport at actinide oxide grain boundaries

Adam Symington
University of Bath, UK

ENVIRONMENTAL CHEMISTRY

Aliovalent actinide incorporation into zirconium(IV) oxide—spectroscopic investigations of defect fluorite structures

Manuel Eibl
Helmholtz-Zentrum Dresden-Rossendorf, Institute of Resource Ecology, Germany

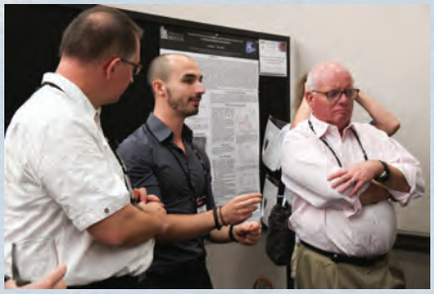

SOLUTION & GAS PHASE CHEMISTRY

Radiolytic recombination of H_2, O_2 and N_2 over PuO_2 and ceramic oxide surrogates

Darryl Messer
Dalton Cumbrian Facility, UK

SURFACE SCIENCE & CORROSION

Modelling the surface chemistry of plutonium dioxide

Jonathan Collard
University of Manchester, UK

Jean-Francois Vigier

Jean-Francois Vigier is a Research Fellow at the European Commission Joint Research Centre (Karlsruhe, Germany). He presented this work at Pu Futures 2018 in Poster Session I.

Actinide Isotopes for Space Applications: Development of Am-241-Based Materials for Radioisotope Power Systems

Jean-Francois Vigier, Karin Popa, Daniel Freis, Rudy J.M. Konings
European Commission, Joint Research Centre (JRC), P.O. Box 2340, 76125, Karlsruhe, Germany

Most of the space probes that have been used to explore the solar system utilize solar panels to power their electronic systems. However, one significant problem is that the further they are from the sun, the weaker the solar power. The solar energy density around Saturn is only 1% of the value received at the surface of Earth, and this energy density drops to just 0.1% around Neptune and Pluto. It is therefore impossible to use solar panels in this part of the solar system, and all such missions launched previously have used radioisotope thermal generators (RTGs) to produce electricity under these conditions. Well-known examples are the Voyager, Cassini, or New Horizons missions. Additionally, RTGs are used in the inner solar system to overcome the problem of long lunar nights (lasting 14 Earth days) or on Martian missions to mitigate the impacts of sandstorms which can block solar panels.

RTGs convert the heat of radioisotope decay directly into electricity using thermocouples based on the Seebeck effect. The isotope of choice to power these generators is ^{238}Pu. With a half-life of 88 years, this alpha-emitter demonstrates a good compromise between significant heat production (567 W/kg) and stable power output during operation time. In addition, it emits low-energy gamma radiation of low activity and therefore does not require heavy shielding. However, this isotope suffers from a global shortage and is very expensive due to its complex production process (Fig. 1).

Americium-241 origin and decay

$$^{241}_{94}\mathrm{Pu} \xrightarrow{t_{1/2} = 14\ \mathrm{yrs}} {}^{241}_{95}\mathrm{Am} + {}^{0}_{-1}\mathrm{e}^{-}$$

$$^{241}_{95}\mathrm{Am} \xrightarrow{t_{1/2} = 433\ \mathrm{yrs}} {}^{237}_{93}\mathrm{Np} + {}^{4}_{2}\alpha$$

Plutonium-238 origin and decay

$$^{237}_{93}\mathrm{Np} + {}^{1}_{0}\mathrm{n} \xrightarrow{\textit{neutron irradiation}} {}^{238}_{93}\mathrm{Np}$$

$$^{238}_{93}\mathrm{Np} \xrightarrow{t_{1/2} = 2\ \mathrm{days}} {}^{238}_{94}\mathrm{Pu} + {}^{0}_{-1}\mathrm{e}^{-}$$

$$^{238}_{94}\mathrm{Pu} \xrightarrow{t_{1/2} = 88\ \mathrm{yrs}} {}^{234}_{92}\mathrm{U} + {}^{4}_{2}\alpha$$

Figure 1. Synthesis of ^{238}Pu requires the production of ^{237}Np, and subsequent irradiation in a nuclear reactor to generate ^{238}Pu by neutron capture and consequent beta decay. Finally, the ^{238}Pu isotope obtained from this irradiation must be extracted from the ^{237}Np by a chemical separation process.

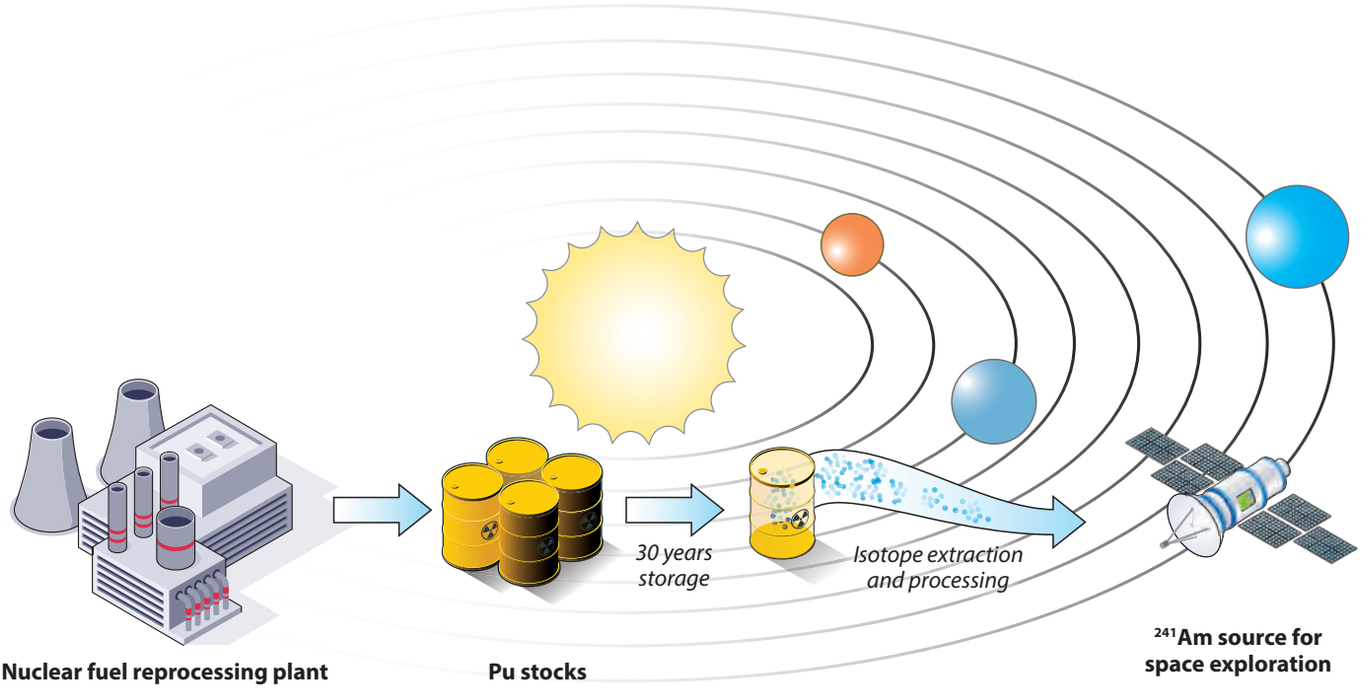

Figure 2. ^{241}Am isotope is a by-product of the nuclear fuel reprocessing industry that could be used as a heat source for radioisotope thermal generators (RTGs) in space probes.

For these reasons, the European Space Agency has decided to explore ^{241}Am as a potential alternative fuel for RTGs despite its lower specific heat (114 W/kg with a half-life of 433 years) and higher gamma activity. This isotope is much more available than ^{238}Pu due to the industrial-scale reprocessing of spent nuclear fuel at facilities such as Sellafield (UK) and La Hague (France). Several tens of tons of separated plutonium are stored in these plants. The plutonium isotope composition depends on the irradiation history of the fuel, but it generally contains about 5% of ^{241}Pu, which progressively converts into ^{241}Am via beta decay with a half-life of 14 years. Therefore, significant quantities of isotopically pure ^{241}Am can be obtained by chemical extraction from aged separated plutonium stocks. Thus, we can gain both a power source for space exploration and purified plutonium free of ^{241}Am, which is considered a neutron poisoning agent for the recycling of used plutonium in nuclear power reactors.

Americium oxides

To be used in a radioisotope power system, americium first needs to be in a stable chemical and mechanical form. This stability has to be preserved under different conditions, namely: standard operations in space, storage on Earth, or re-entry during an accident. The first choice of material is an americium-oxygen based solid. Two preparative strategies could then follow:

Oxidative sintering to produce a ceramic of cubic AmO_2 oxide. During operation at high temperatures in the vacuum of space this material would, however, be expected to release oxygen. In this process, the ceramic would be initially reduced to AmO_{2-x}, which is linked to significant material swelling. The total reduction of this oxide into hexagonal Am_2O_3 sesquioxide is then responsible for a phase transformation that can further damage the ceramic.

Reductive sintering to produce a ceramic of hexagonal Am_2O_3 sesquioxide. In this case, the anisotropic dilation of the material can induce internal strain which makes the sintering itself difficult and can produce cracks in the ceramic.

Table 1. Power densities of different americium materials, and comparison to $^{238}PuO_2$.

Actinide oxide	PuO_2	AmO_2	Am_2O_3	$AmAlO_3$	$AmPO_4$	$(Am_{0.80}U_{0.12}Np_{0.06}Pu_{0.02})O_{1.8}$
Power density, W/kg	425*	101	104	87	82	82

* considering ^{238}Pu having an 85% isotopic purity.

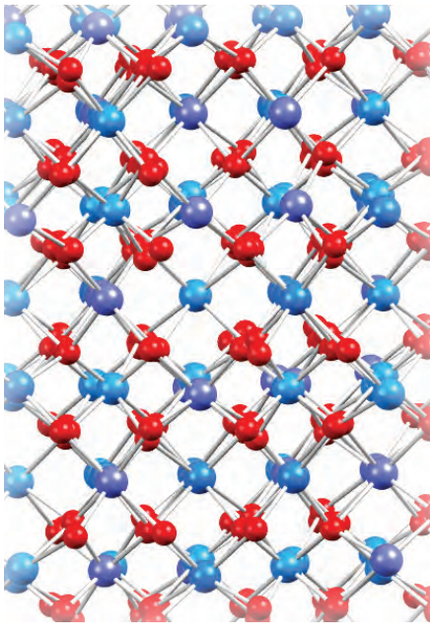

Figure 3. Crystallographic structure of uranium-doped americium oxide. Americium, uranium, neptunium (daughter element of americium), and plutonium (impurity coming from initial americium reprocessing) share the same crystallographic position, which shows the chemical flexibility of this material.

Furthermore, the produced material would be sensitive to oxidation during storage or in the event of accidental damage or atmosphere breach. Such oxidation converts the material into cubic AmO_2 which would lead to degradation and disintegration of the ceramic.

Thus, binary americium oxides are not stable enough for this application (Fig. 5). Alternative materials were therefore studied for the production of stable americium ceramics. The desired characteristics are: high americium density (Table 1), stability under a range of oxidative and reductive conditions, and resistance to self-irradiation damage.

Americium aluminate ($AmAlO_3$)

This material displayed good resistance to oxidation; however, it showed significant swelling under self-irradiation followed by amorphization (Fig. 4). Furthermore, due to a strong (α,n) reaction with the aluminum atoms, it is a significant neutron source which could cause radioprotection issues during handling.

Americium phosphate ($AmPO_4$)

As with americium aluminate, this material also shown good chemical stability. Crystallographic swelling was more moderate than for the aluminate, but it also showed an amorphization under self-irradiation.

Doped americium oxide ($(Am,U)O_{2-x}$)

This more complex material showed promising results for the production of stable ceramics. Using uranium as a dopant, the cubic phase of americium oxide was stabilized even during reductive sintering of the material (Fig. 3), solving the various problems of phase transformation described above for pure americium oxides. The stabilized phase is a fluorite-related structure, which is known to have excellent resistance against self-irradiation, due to its ability to accommodate disorder. The material obtained in this way indeed kept crystallinity under self-irradiation and showed a limited crystallographic swelling of 0.4 vol.%.

Following the promising results obtained with uranium-doped americium oxide, a large ceramic pellet of this material was prepared for a small-scale radioisotope heater unit prototype. A pellet of 2.96 g of stabilized americium oxide containing 2.13 g of ^{241}Am was produced (Fig. 6a). The material showed desirable behavior during sintering—there were no structural changes at high temperature, and the preservation of the cubic structure during the whole thermal cycle ensured anisotropic thermal dilatation, limiting internal strain in the material during the cooling step.

The americium used in this study had been aged for approximately 40 years and therefore contained a significant amount of ^{237}Np due to the alpha decay of ^{241}Am. It also contained a small amount of plutonium originating from the initial reprocessing of the americium. After sintering, an elemental scan was performed

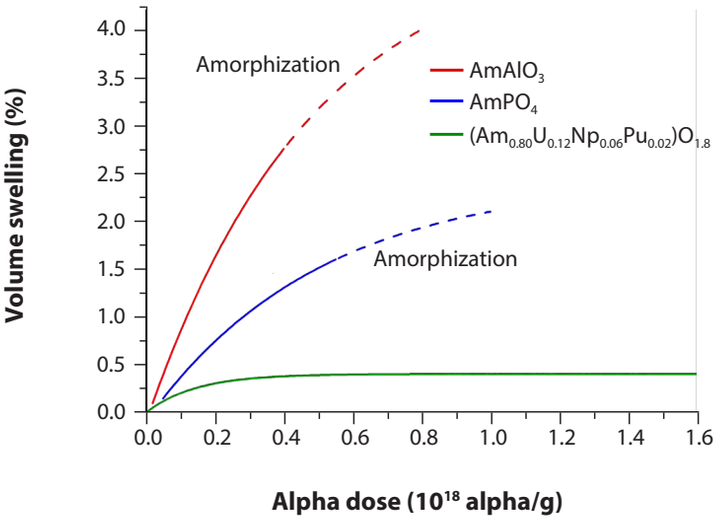

Figure 4. Crystallographic swelling of several americium compounds as function of alpha dose followed by X-ray diffraction. The dashed lines represent amorphization, i.e., decomposition of the crystal structure. This graph shows undesirable swelling with increasing alpha radiation dose for americium aluminate ($AmAlO_3$) and phosphate ($AmPO_4$). Doped americium oxide ($(Am_{0.80}U_{0.12}Np_{0.06}Pu_{0.02})O_{1.8}$) meanwhile shows good stability with minimal swelling in this test.

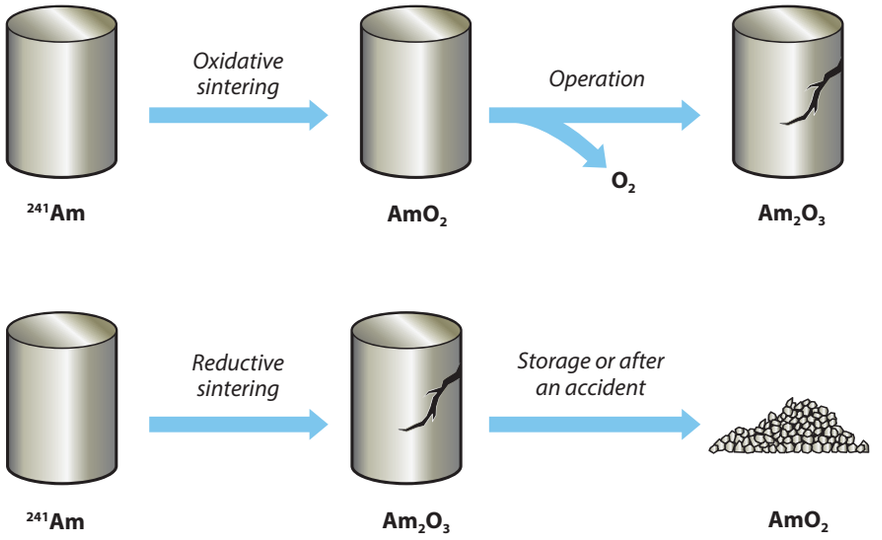

Figure 5. Challenges with pure americium oxide ceramics manufacturing for radioisotope power systems. AmO_2 ceramics are unstable at high temperature under the vacuum of space and convert into Am_2O_3 during operation. Am_2O_3 ceramics are sensitive to oxidation and can convert into AmO_2 if exposed to oxygen. Phase changes are generally linked to ceramic damages.

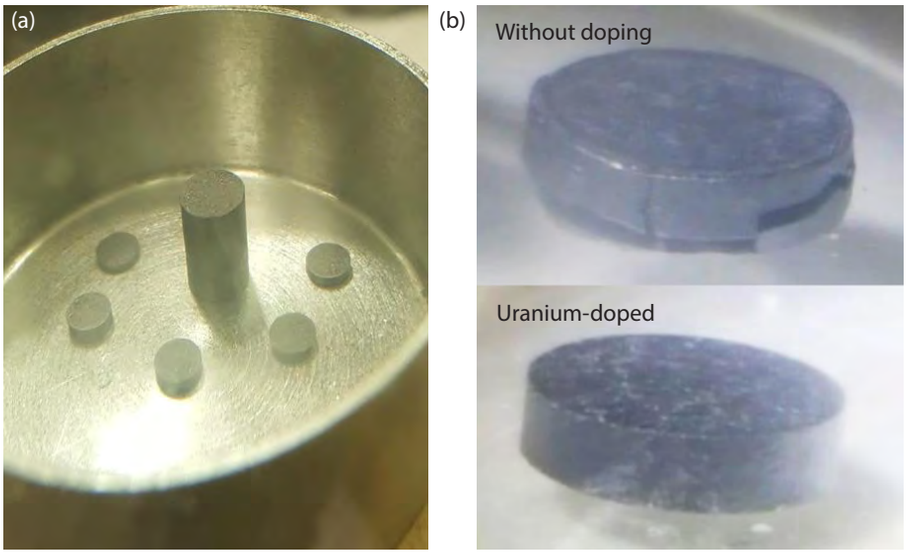

Figure 6. (a) Photograph showing pellets after sintering of uranium-doped americium oxide, which were prepared for a small-scale radioisotope heating unit prototype (2.96 g weight, 10.53 mm height, 6.00 mm diameter, 93%TD, 2.13 g of ^{241}Am, 243 mW decay heat). (b) The initial composition of the discs were (top) hexagonal Am_2O_3 and (bottom) cubic $(Am_{0.80}U_{0.12}Np_{0.06}Pu_{0.02})O_{1.8}$. These photographs show the effect of oxidation with air at 1000°C on the integrity of the discs for the two types of materials.

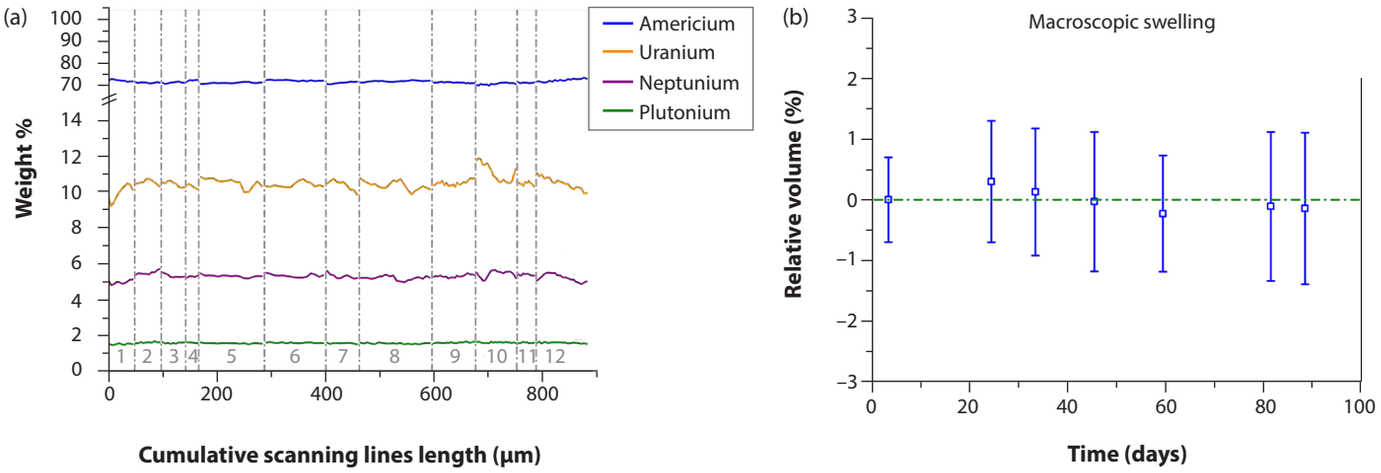

Figure 7. (a) Elemental analysis of a uranium-doped americium oxide sample cross-section at twelve different depths (as indicated by dashed lines). This data shows the homogeneous distribution of different actinides within the material. (b) Volume variation of this material in pellet form over time, relative to its initial measurement. This shows good stability with respect to macroscopic swelling.

on a polished sample of the material and showed a homogenous distribution of the different actinide ions in the material (Fig. 7a). This confirms that the cubic structure is chemically flexible and is a good host for neptunium, which forms a solid solution with $(Am,U)O_{2-x}$ mixed oxide. This property is encouraging for the long-term behavior of the material.

Material stability tests

The macroscopic swelling behavior of $(Am_{0.80}U_{0.12}Np_{0.06}Pu_{0.02})O_{1.8}$ has also been examined. Material expansion is an important issue for materials with high alpha activity, and the amount of macroscopic swelling can far exceed crystallographic swelling. However, no significant swelling of the uranium-stabilized americium pellet was measured (Fig. 7b), suggesting good behavior of the material under alpha self-irradiation.

Finally, oxidation tests were performed on both americium sesquioxide and uranium-doped americium oxide discs. In contrast to Am_2O_3, the integrity of the $(Am_{0.80}U_{0.12}Np_{0.06}Pu_{0.02})O_{1.8}$ disc was preserved during the test (Fig. 7b). This stability is attributed to the minimal amount of structural reorganization during the oxidation process, since the oxidized and reduced phases both have a cubic fluorite or fluorite-related structure. This highlights improved resistance of the material to leakage of radioactive solids compared with Am_2O_3, in the case of accidental damage (e.g., an oxygen leak).

Summary

Uranium doping for americium oxide ceramic manufacturing has led to a number of improvements of the material. These include improvements of the long-term behavior during decay product growth, sinterability, stability under self-irradiation, and stability at elevated temperatures and oxygen potentials, e.g., during accidental oxidative conditions. Uranium-doped americium oxide shows potential as a host material for ^{241}Am. Therefore, despite its higher gamma radiation and lower specific power density, ^{241}Am seems to be a credible alternative to ^{238}Pu as a radio-isotope power source for space applications.

Acknowledgments

The authors gratefully acknowledge Antony Guiot, Sébastien Gardeur, Patrick Lajarge, Daniel Bouëxière, Damien Prieur, Philipp Pöml, and Jerome Himbert for their help during experimental work and the fruitful discussions.

In Stream Monitoring of Off-Gasses from Plutonium Dioxide Fluorination

Amanda Casella,[1] Jennifer Carter,[1] Amanda Lines,[1] Job Bello,[2] Sam Bryan,[1] Richard Clark,[1] Jordan Corbey,[1] Calvin Delegard,[3] Forrest Heller,[1] Bruce McNamara,[1] Lucas Sweet[1]

Fluorination of actinides and lanthanides is an important step in the process of obtaining high purity metals. For both uranium and plutonium metal production, reduction reactions are performed using their corresponding tetrafluorides, UF_4 and PuF_4, with Ca metal. Uranium tetrafluoride itself can be treated with fluorine gas to produce the semi-volatile uranium hexafluoride, UF_6, for use in uranium isotope enrichment. Fluorinated actinides are also utilized in molten salt reactors. These systems can contain UF_4, PuF_3, and ThF_4 as fuels and blanket salts; U-238 fluorides meanwhile can be transmuted to fluorinated plutonium, neptunium, americium, and curium products.

Preparation of both UF_4 and PuF_4 is typically achieved by reacting hydrogen fluoride gas (HF) with the respective dioxides, UO_2 and PuO_2. This fluorination reaction (Reaction 1) was used for plutonium metal production in the United States, although other fluorinating agents have been investigated.

Technology enabling real-time analysis is currently being developed to assess and improve processes used for the fluorination of actinides, creating materials which have increasing importance in nuclear forensics and molten salt reactor applications. The well-established fluorination method uses HF, a toxic and corrosive gas, which greatly limits what materials can be used for probes and interfaces, as they are typically incompatible with detectors at greater than part per million (ppm) concentrations. In our work, new methods are being developed to provide instantaneous process information about the off-gas stream in conditions up to 100% HF. The real-time data not only provides reaction information but also reduces the use of HF via process optimization, improving worker health and safety, minimizing waste, and prolonging equipment life.

Fluorination reactions

Anhydrous HF fluorination of PuO_2 produces both PuF_4 and PuF_3. Reaction 1 is typically run with O_2 present to prevent Reaction 2, the unwanted reduction to PuF_3 from H_2 impurities that are generally present in commercial HF. The additional O_2 reacts with H_2 to produce H_2O and therefore prevents this side reaction from occurring.

(1) $PuO_2 + 4HF \longrightarrow PuF_4 + 2H_2O$

(2) $PuO_2 + 3HF + \frac{1}{2}H_2 \longrightarrow PuF_3 + 2H_2O$

[1] *Pacific Northwest National Laboratory, Richland, WA 99352;* [2] *Spectra Solutions, Norwood, MA 02062;* 3 *TradeWind, LLC, Richland, WA 99352.*

Amanda Casella

Dr. Casella is a Research Engineer at Pacific Northwest National Laboratory. She presented her talk "In Stream Monitoring of Off-Gasses from Plutonium Fluorination" *in the Coordination Chemistry II technical session at Pu Futures 2018.*

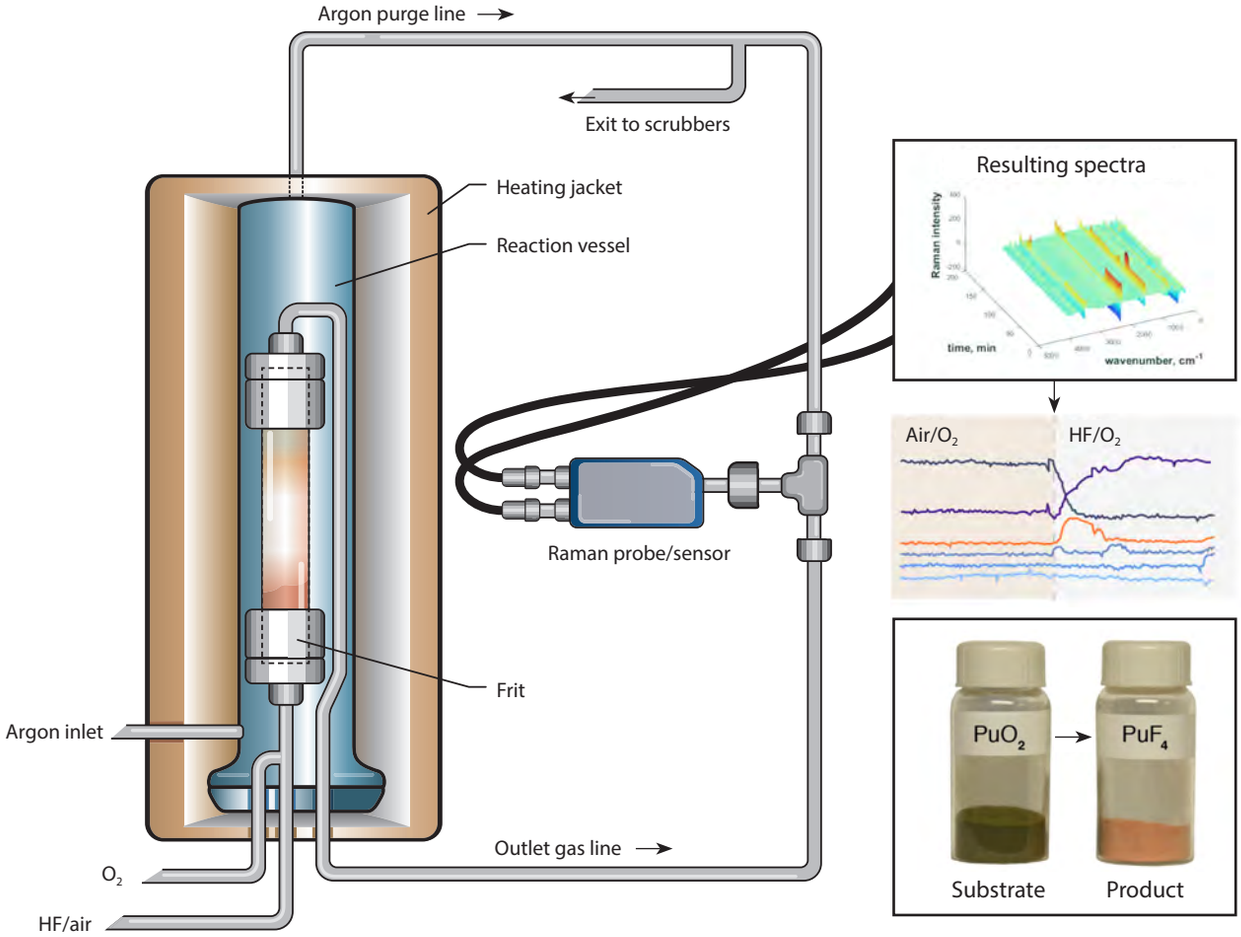

Figure 1. Schematic of fluorination apparatus with real-time monitoring of off-gasses by Raman spectroscopy. This apparatus allows for two gas combinations, air/O_2 or HF/O_2, to enter through separate streams at the base of the column and flow upwards through the PuO_2 bed. The input was air/O_2 initially then switched to HF/O_2 at 300°C. The off-gas stream then exits the system, sweeping the H_2O product. An outer housing with an argon purge was fitted over the column to divert potential HF leaks to an abatement system and prevent corrosion in the radiological glovebox. Upon exiting the reaction column, the off-gases pass by the in-situ fiber-optic Raman probe. Spectral measurements of the off-gas stream were performed using a Raman system (Spectra Solutions Inc.) which optically couples the Raman probe to the Raman spectrometer by a fiber-optic cable.

Methods for monitoring fluorination reactions

A real-time analysis technique is desirable to monitor these and similar actinide reactions with HF or other potential fluorinating agents. Neutron dose monitoring is a viable method to track the plutonium reactions, as neutrons arise from the alpha particle interaction with the fluorine. However, the signal strength indicating the extent of reaction is complicated by the quantity of material reacted, distance of probe from source, and interference of background neutron emitters. This method would also be less effective for other actinides, such as uranium, which have lower alpha decay rates. An alternative method would be downstream in-situ monitoring of HF. This technique is difficult as anhydrous HF gas is corrosive and incompatible with many materials in common detection systems. Standard HF detectors used for worker health and safety monitoring have a maximum concentration range of 9 to 40 ppm, requiring significant dilution.

Raman spectroscopy was identified as an optimal technique for downstream HF gas monitoring, as a cell can be fabricated to withstand the harsh environment of up to 100% HF. This technique keeps the probe outside the stream, while the laser can be focused inside the off-gas flow via an HF-resistant transparent window. Vibrational spectroscopy also allows monitoring of other gases such as the reaction product H_2O and CO_2 (from incomplete conversion if there is an oxalate precursor or if surface-sorbed CO_2 is present), N_2 and O_2 from the environment, and H_2 from the headspace of the HF cylinder, providing more insight into the reaction process.

Experimental procedure

The fluorination apparatus is described in Fig. 1. A typical run consisted of the following steps. PuO_2 was heated to 300°C in air and additional O_2 necessary to counter H_2 built up in the headspace of the HF cylinder, was then introduced to sustain forward flow in the inlet lines. Once the temperature stabilized, the flow was switched to HF (O_2 flow maintained), and the temperature was increased to 480°C and held until a sharp increase in HF concentration—known as the "HF breakthrough"—was observed, indicating near-completion of the fluorination reaction. The HF flow was continued for an additional interval to ensure complete conversion of the PuO_2. The heater was then turned off, returning the system to room temperature. The gas inlet was switched from HF to air when the vessel reached around 200°C.

Results

The real-time Raman spectroscopic data for the first run are shown in Fig. 2. The reaction completion was indicated by the HF breakthrough, shown by the black dashed line. N_2 and O_2 were observed in the initial air environment; the N_2 concentration decreased when the air supply was switched off and the HF turned on, as would be expected.

H_2 was detected when the gas inlet was switched to HF, indicating that the level of O_2 in the system initially was insufficient to convert H_2 to H_2O. The H_2 levels decreased, or were eliminated (depleted from the HF bottle headspace) prior to the end of the experiment. CO_2 was also observed when the gas stream was switched to HF. While this could have been present in the headspace of the HF bottle, it most likely arose from either oxidation of residual Pu(IV) oxalate (left over from the calcination to produce PuO_2) or CO_2 sorbed on the PuO_2 surface. This conclusion is supported by observations showing recurrences of the peak during multiple fluorination runs and a comparison with a blank run with no plutonium in the vessel. A second release of CO_2 was observed when the maximum temperature of 480°C was achieved. However, this may be an effect of temperature or H_2 as it closely corresponds to the disappearance of the H_2 band. The H_2O product from the reaction was not readily observed in this run, which may be related to weak signal strength/low concentration but is more likely caused by a reaction with the Inconel lines between the reaction vessel and spectroscopy cell, as supported by observations in the following experiments.

A complication occurred during the 185–280 minute period which resulted in the loss of useful spectroscopic data. The spectral baseline increased and eventually became saturated after the HF breakthrough. The baseline increase was likely caused by fluorescence from corrosion products deposited on the backside of the Inconel flow cell. It was determined that this fluorescence background could be minimized by maintaining higher temperatures in the cell, thus preventing data loss in future runs.

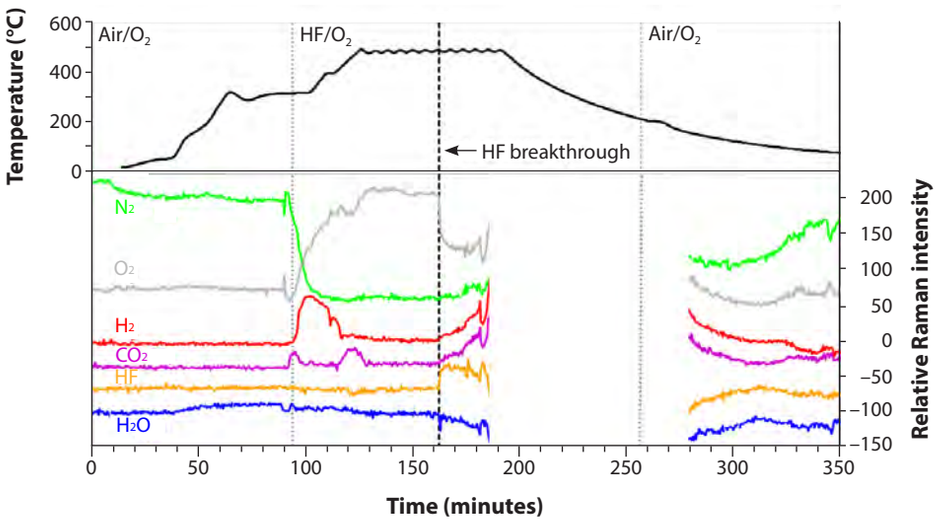

Figure 2. Thermal profile and processed Raman data for peaks associated with N_2, O_2, H_2, CO_2, HF, and H_2O recorded during the first fluorination experiment using PuO_2. Background fluorescence likely caused by corrosion products caused the loss of spectral data for the 185–280 minute period. The data are offset in intensity to increase clarity (also in Fig. 3).

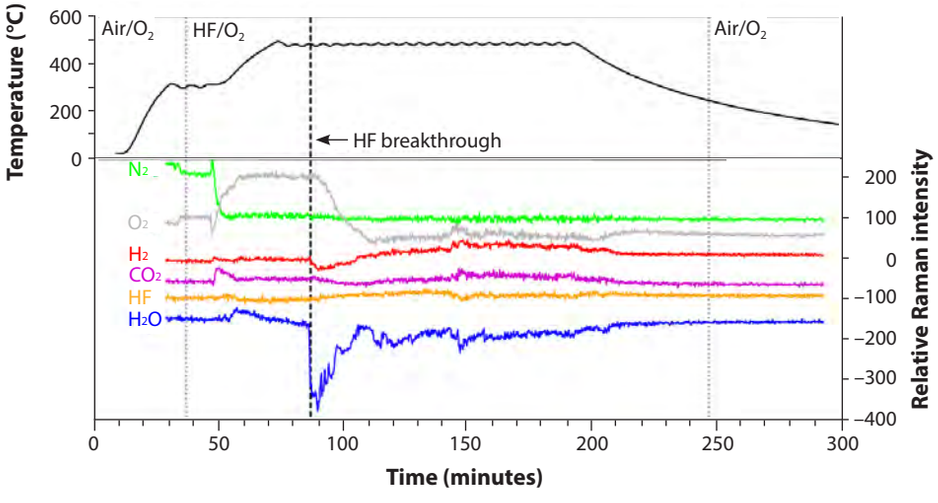

Figure 3. Data as per Fig. 2 for the second fluorination experiment using PuO_2, which was optimized by increasing the amount of O_2 and heating the outlet gas line to approximately 100°C to reduce background fluorescence.

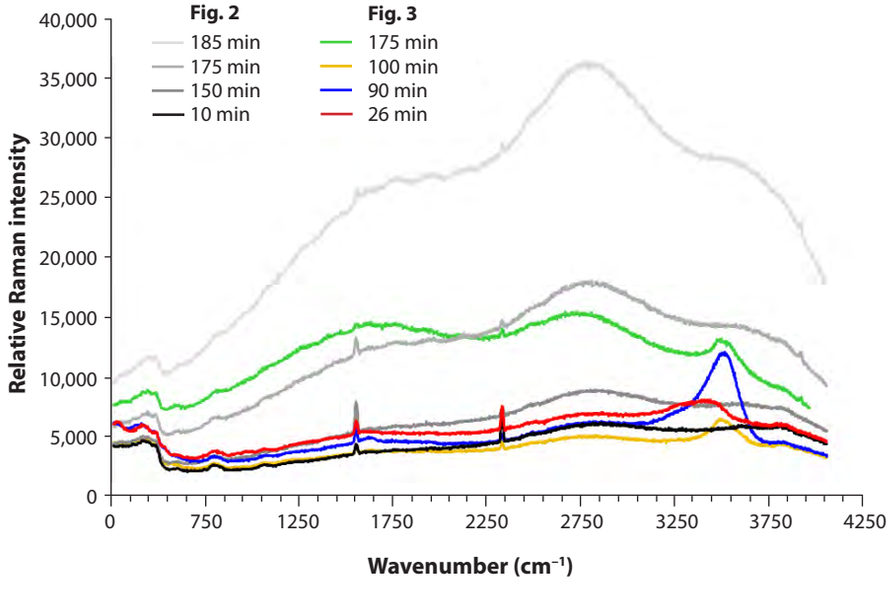

Figure 4. Unprocessed Raman spectra from the initial run with Raman signal saturation (grayscale) and second run with additional applied heating on effluent lines (colored, recorded at 100°C) representing timestamps before and after HF breakthrough in the column. The peaks at approximately 1650, 2850, and 3550 cm^{-1} are attributed to a water reaction with the Inconel on the back of the cell.

Refinement of parameters

The product from this run contained 99 wt.% PuF_4 and 1 wt.% PuF_3 (the PuF_3 side-product being produced by Reaction 2) as deduced by Rietveld refinement of the X-ray diffraction pattern. Subsequent runs were optimized by increasing the amount of O_2 relative to HF in order to inhibit the formation of PuF_3. Heating the outlet gas line to approximately 100°C prevented spectral saturation from the fluorescence background, thus allowing real-time data to be collected for the entirety of the run. With these improvements, and a similar thermal profile (Fig. 3), complete conversion to PuF_4 occurred, as validated by X-ray diffraction studies. Minimal changes in the H_2 band were observed when the HF stream was turned on. Other gases monitored remained at similar levels to the previous run.

Water reactions causing corrosion side-product

In both runs, a significant drop in the intensity of the water peak occurred simultaneously with HF breakthrough. This decrease most likely arose from water/HF reaction with the Inconel lines and Raman cell, as was observed in the fluorescence in the Raman spectra. The grayscale data in Fig. 4 show the unprocessed spectra from the first run at various times and right before signal saturation (greater than 40,000 relative to the Raman intensity). In these spectra, the ingrowth of broad fluorescence bands roughly centered at 1650, 2850, and 3550 cm^{-1} was observed. This fluorescence background results from a species forming on the backside of the Inconel cell containing the Raman window. The effect on the spectra of increasing the cell temperature to 100°C is shown in the colored data in Fig. 4, decreasing background by about a factor of two. In these spectra, the increased temperature not only suppressed the growth of the fluorescence peaks, but also changed the ratio between them indicating an alteration in the products formed. While it was not the focus of this study, this data highlights an opportunity for further investigation into the reactivity of corrosion product composition and buildup rates.

Summary

We achieved improvements in the monitoring of the production of fluorinated plutonium compounds (and potentially other actinide fluorides) via development of a novel in-situ Raman system capable of monitoring off-gas products in a corrosive environment of up to 100% anhydrous HF gas. A series of experiments were performed to produce PuF_4 from PuO_2, with real-time data collected for HF, environmental gases (O_2 and N_2), off-gas products (H_2O, CO_2), and trace components from the HF gas cylinder (H_2). This can be utilized to more accurately characterize and tailor actinide fluorination reactions. In addition, we have discovered a new approach to investigate corrosion product build-up on system materials during fluorination processes.

Acknowledgments

The fluorination capability and material conversion efforts were internally supported by the National Security Directorate at Pacific Northwest National Laboratory (PNNL), a multiprogram national laboratory operated by Battelle for the U.S. Department of Energy. The real-time reaction analysis was supported by the Office of Defense Nuclear Nonproliferation Research and Development within the U.S. Department of Energy's National Nuclear Security Administration and PNNL, which is operated by Battelle Memorial Institute for the U.S. Department of Energy under contract DE-AC05-76RLO1830. Image used in Fig. 1 is based on one created by Rose Perry of the PNNL Creative Services Group.

Dallas Reilly presented this work in a talk titled *"A New Paradigm in Actinide Research: Nuclear Materials Science at the Micron-Scale"* at Pu Futures 2018.

Jon Schwantes

Dr. Schwantes is a Senior Scientist at Pacific Northwest National Laboratory with over 20 years of experience as a radiochemist. Dr. Dallas Reilly gave his talk at Pu Futures 2018 in his place during the Metallurgy and Materials Science II technical session.

Nuclear Materials Science at the Micron Scale

Jon Schwantes,[1] Dallas Reilly,[1] Richard Clark,[1] Daniel Perea,[1] Richard Buckner,[1] Richard Pierson,[1] Edgar Buck,[1] John Cliff,[1] Michele Conroy,[1] Timothy Lach,[1] Paul MacFarlan,[1] Sue Clark,[1] Reid Peterson,[1] J. David Robertson,[2] Camille Palmer,[3] Todd Palmer[3]

Pacific Northwest National Laboratory (PNNL) has developed a new concept of operations at the Radiochemical Processing Laboratory (RPL), our Hazard Category II Nuclear Facility, for preparing nuclear and radioactive samples that may alter the manner in which nuclear materials science is conducted in the future. This concept of operations, known as the "Free Release Workflow" process, relies on an FEI Helios NanoLab 660 dual focused ion beam (FIB) and scanning electron microscope (SEM) to prepare sub-micron-scale samples. In this manner, macro quantities of actinide solids or highly radioactive materials typically requiring glovebox operations or hot cell facilities can be sub-sampled using an FIB to activity levels that fall below the Department of Energy's (DOE's) radiological clearance limit. These micron-sized specimens can then be "released" from the nuclear facility and transferred to other facilities on campus, even non-radiological laboratories, with appropriate controls. This process also reduces the radiological control requirements for off-site collaborators by reducing the sample inventory, which creates opportunities for further experimentation and analysis.

Conducting nuclear materials analysis at the micron scale offers a number of advantages over the bulk scale, including:

- Access to instruments that are not dedicated to radiological work.
- Reduction of risk to the scientist(s) by minimizing radiation exposure and dose.
- Reduction/elimination of the need for specialized laboratories and facilities.
- Increased accessibility of these materials to a broader scientific community.
- Waste minimization.

Micron scale allows in-depth analysis at non-radiological facilities

A variety of materials have been prepared at the RPL using the Free Release Workflow process. These sub-samples have subsequently been transferred out of the RPL to low- and non-radiological facilities across and off campus for follow-on experiments and specialized analyses. For instance, micron-sized sub-samples of highly-enriched uranium metal and oxide fuel samples have been analyzed by secondary ion mass spectrometry (using both large-geometry and nano techniques), aberration-corrected transmission electron microscopy (TEM), nano-commuted tomography (CT), and atom probe tomography (APT), to investigate the persistence of isotopic heterogeneities and the presence of inclusions (Fig. 1a,b). The majority of these high-end instruments are not dedicated to radiological work and reside within the DOE's national user facility, the Environmental and Molecular Sciences Laboratory (EMSL), a non-radiological facility. Sub-samples of plutonium metal produced via bomb reduction at the RPL were also prepared and successfully analyzed by APT—the first known report using this analytical technique on this type of material (Fig. 1c,d).

[1] *Pacific Northwest National Laboratory, Richland, WA 99352;* [2] *University of Missouri, Columbia, Missouri 65201;* [3] *Oregon State University, Corvallis, Oregon 97331.*

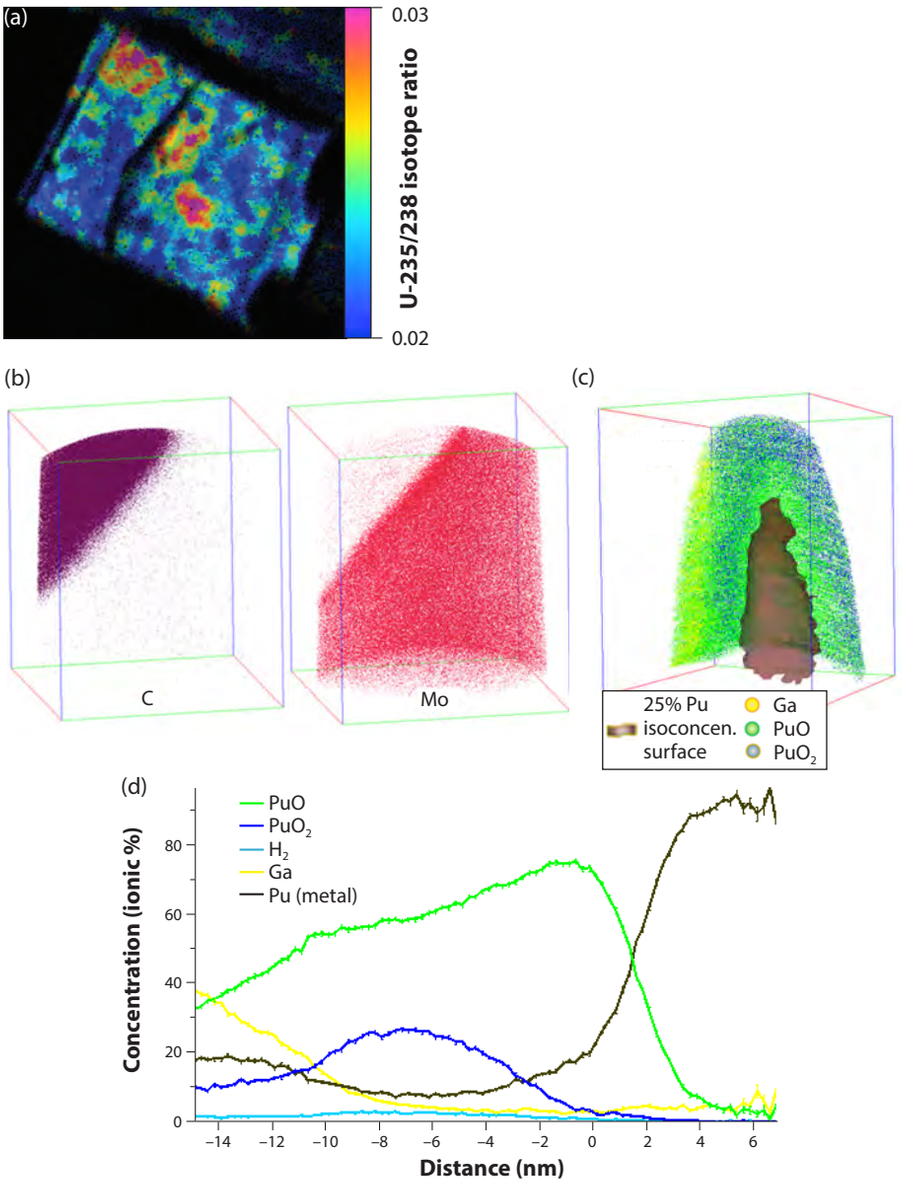

Figure 1. (a) Nano-SIMS (secondary ion mass spectrometry) analysis of UO_2. (b) Atom probe tomography (APT) analyses of a U/Mo metal fuel sample, showing the boundary of the metal alloy and carbide inclusion. This data demonstrates the structural insight that can be gained at the sub-micrometer scale with these techniques. (c) and (d) APT data for a submicron sample of Pu metal. This is the first known report using this analytical technique on this type of material.

The Free Release Workflow process has also been used to facilitate cost-effective studies to avoid the need for specialized glovebox or hot cell facilities. As an example, micron-sized samples of un-irradiated UO_2 fuel were prepared at PNNL and shipped to the University of Missouri's Research Reactor (MURR) for irradiation studies (Fig. 3). Prior to shipping, samples were attached to commercially-available TEM half-grids via ion deposition, which were then housed in specially-designed aluminum sample holders approved for use at the reactor facility. In this manner, samples were ready to be analyzed without further preparation following irradiation. Additionally, by conducting irradiation experiments at the micron-scale, post-irradiation cooling times prior to analysis were reduced and handling of these samples was permitted outside of a hot cell facility.

Spent fuel analysis

The utility of the Free Release Workflow has been further exemplified in the preparation and analysis of noble metal phase particles in used nuclear fuel (Fig. 4). Here, used fuel residing in the RPL's hot cell facility was macroscopically sub-sampled

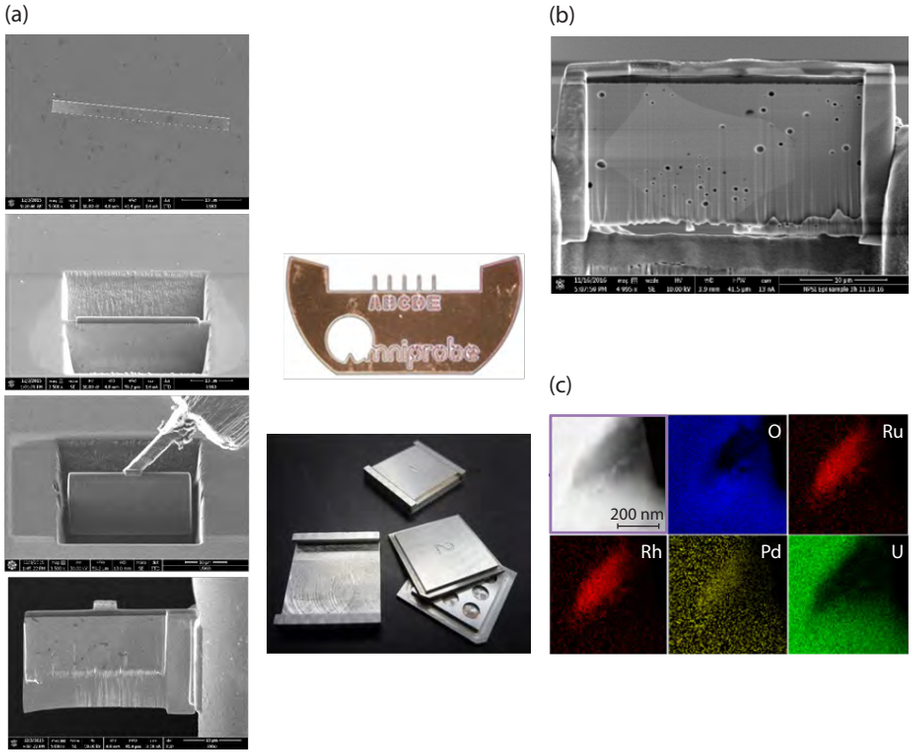

Figure 3. (a) Preparation of UO_2 by FIB for micron irradiation studies at MURR. (b) Scanning electron images of one of the samples after irradiation. (c) Elemental map of an irradiated micron-sized sample of UO_2 showing the presence of noble metal phase particles.

Part of the research team responsible for applying the Free Release Workflow process at PNNL to study noble metal phase particles in used nuclear fuel. *Left to right, front row*: Kerry Garrett, Daniel Parea, Edgar Buck, Paul MacFarlan, Michele Conroy, Kristi Pellegrini, Chuck Soderquist; *Back row*: Sean Kessler, Jamin Trevino, Richard Clark, David Abrecht, Jon Schwantes.

by remote manipulation to reduce sample activity to a level that could be transferred out of the hot cell (< 1 Ci) and to the FIB for further sectioning. Samples were subjected to a variety of electron imaging and micron/sub-micron sectioning processes for further analyses by TEM and APT, both located at other campus facilities. The smallest of these sub-samples, needles prepared for APT analysis, represented a 1017-fold reduction in size and activity of the starting materials (a full-length fuel rod) to a level of activity transferable from the Category Level nuclear facility to EMSL, a non-radiological facility, for analysis on a corresponding non-radiological instrument. This sample size reduction is roughly equivalent to reducing an area the size of Asia down to that of a penny.

A novel yet conservative approach was developed to manage the potential accumulation of activity over time on instruments not specifically dedicated to radiological work. This accounting tracks the total accumulated activity on each instrument by conservatively assuming 100% of the destroyed portion of the sample's mass is deposited within the instrument during analysis. Once the total accumulated activity calculated for that instrument reaches a certain percentage of the radiological clearance limit, that instrument is no longer available to run radioactive samples. Depending upon the specific activity and nature of the radioactive material, this approach generally provides the ability to analyze 100s to 10,000s of samples prepared by the Free Release Workflow process on an individual instrument without concern for exceeding these limits. To illustrate the level of radioactivity the Free Release Workflow is designed to manage, consider the analysis of surface soil, which contains a miniscule amount (~10–13 Ci/g) of Pu from global fallout. An environmental laboratory that analyzes just 20 one-gram soil samples a day could theoretically accumulate enough Pu within their instrument to exceed the DOE's radiological clearance limits in 50 work days.

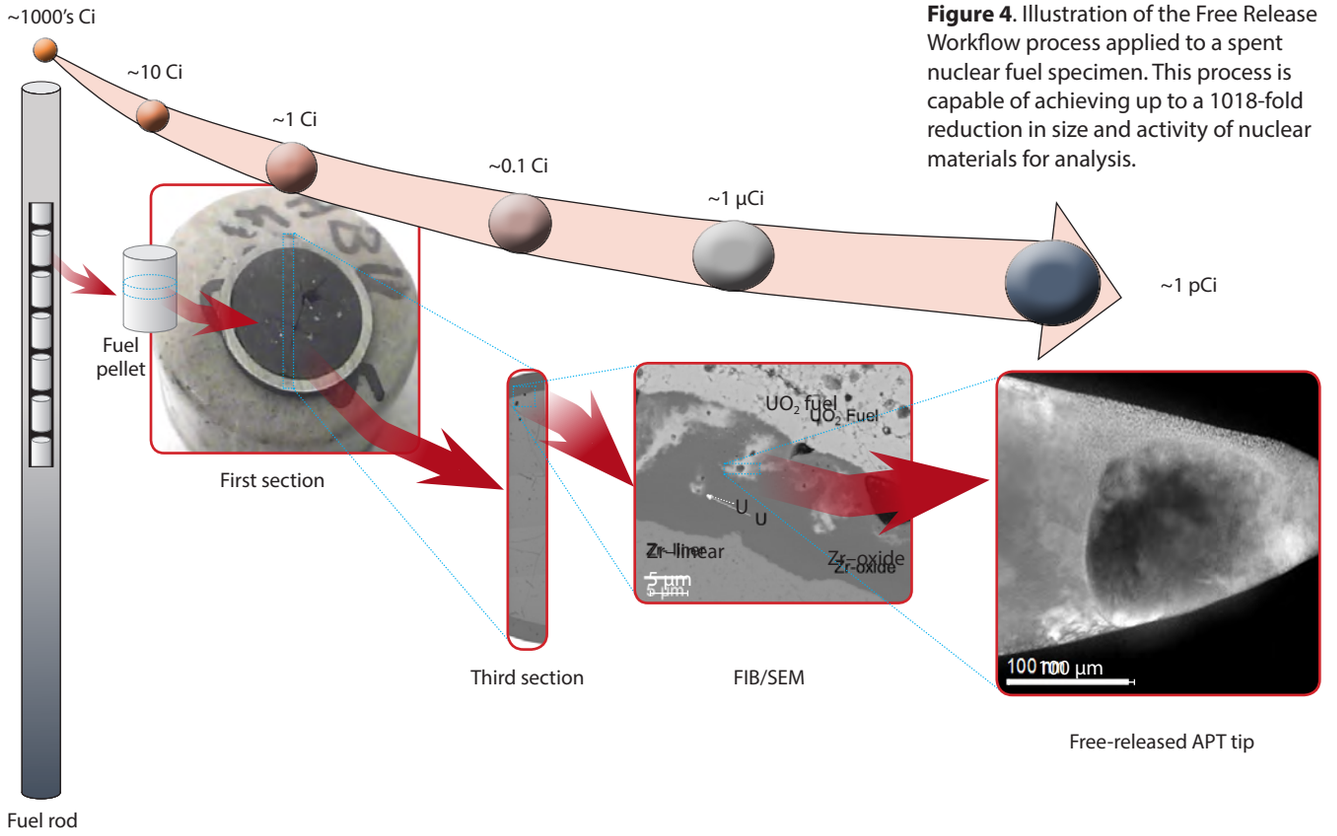

Figure 4. Illustration of the Free Release Workflow process applied to a spent nuclear fuel specimen. This process is capable of achieving up to a 1018-fold reduction in size and activity of nuclear materials for analysis.

Summary

The overall vision of the Free Release Workflow process at PNNL is to enhance collaboration and accessibility of nuclear materials science to the broader research community, enhance accessibility of cutting edge research tools, techniques and technologies to the nuclear science community, lower the risk to the scientist by reducing radiation dose and exposure, reduce facility and research costs associated with conducting nuclear materials science, and minimize the generation of radioactive waste.

Further Reading:

1. *R.A. Clark, R. Devanathan, E.C. Buck, M.A. Conroy, T.C. Droubay, K.E. Garrett, W. Jiang, S.H. Kessler, E.J. Krogstad, K. Kruska, T.G. Lach, N.R. Overman, K.L. Pellegrini, J.M. Schwantes, S.D. Shen, C.Z. Soderquist, "Distribution of Metallic Fission Product Particles in the Cladding of Spent Nuclear Fuel", Mat. Deg., accepted.*
2. *T.G. Lach, R.A. Clark, M.A. Conroy, K.L. Pellegrini, E.C. Buck, P.J. MacFarlan, B.K. McNamara, J.M. Schwantes, "Distribution of Fission Product Noble Metal Phase Particles in the Cladding of Spent Nuclear Fuel: evidence for a new mechanism for cladding corrosion", J. Nucl. Mat., 2019.*
3. *K.L. Pellegrini, C.Z. Soderquist, S.D. Shen, E.J. Krogstad, C.J. Palmer, K. Gerez, E.C. Buck, T.G. Lach, M.A. Conroy, J.M. Schwantes, R.A. Clark, "Chemical and Isotopic characterization of noble metal phase from commercial UO_2 fuel", Anal. Chem., 2019, 91, 6522.*
4. *W. Jiang, M.A. Conroy, K. Kruska, M.J. Olszta, T.C. Droubay, J.M. Schwantes, C.A. Taylor, "In-situ Study of Particle Precipitation in Metal-doped CeO_2 during Thermal Treatment and Ion Irradiation for Emulation of Irradiating Fuels", J. Phys. Chem. C., 2019, 123, 2591.*
5. *D.D. Reilly, M.T. Athon, J.F. Corbey, I.I. Leavy, K.M. McCoy, J.M. Schwantes, "Trace Element Migration During UF_4 Bomb Reduction: Implications to Metal Fuel Production, Worker Health and Safety, and Nuclear Forensics", J. Nucl. Mat., 2018, 510, 156.*

Acknowledgments

This work was performed at PNNL in partnership with Oregon State University and the University of Missouri at Columbia and was supported by the Laboratory Directed Research and Development and Nuclear Processing Science Initiative. We thank hot cell technician, Mr. Jamin Trevino, for helping to obtain the polished cross-sections of the ATM-109, Ms. Fran Steen for enabling access to the Shielded Analytical Facility for preparing fuel samples, and the Radiation Protection Technologists in the Radiochemical Processing Laboratory for supporting the work. Dr. Brady D. Hanson kindly provided the specimens of ATM-109 spent fuel and the details of its history.

R. Gian Surbella

Dr. Surbella is a Linus Pauling Fellow at Pacific Northwest National Laboratory (PNNL). He presented his talk "Plutonium Chlorides: A Platform to Explore Assembly, Structure and Bonding" *in the Coordination Chemistry I technical session at Pu Futures 2018. Dr. Surbella is a former student of Prof. Cahill's and has worked to continue this research, in particular with transuranic synthesis and crystallography.*

Professor Christopher Cahill is the principal investigator who led this work and a research group at the George Washington University. Prof. Cahill's broader research agenda is to explore the structural chemistry, properties, bonding, and electronic structure of actinide-containing materials, an effort that is supported by a collaboration with PNNL, the Institute of Chemistry at The University of São Paulo, and the University at Buffalo.

Plutonium Hybrid Materials: Supramolecular Assembly and Bonding

R. Gian Surbella,[1] Christopher L. Cahill[2]

Actinide chemistry remains central to the nuclear arena as legacy efforts to produce nuclear weapons have given way to large-scale endeavors to remediate former nuclear weapons fabrication sites, decommission nuclear weapons materials, and develop long-term strategies for the disposition of used nuclear fuels. Whereas significant strides are being made in each area, there remain non-trivial technical hurdles that impede progress, many of which were at the forefront of the scientific program at the 2018 Plutonium Futures conference held this past September. The technical presentations touched upon such issues while highlighting the most recent advances in actinide chemistry (including plutonium of course!), yet ultimately the lectures provided a forum for forward-looking conversations regarding the most pressing scientific challenges facing the actinide community. In particular, the role of the 5f electrons in the unique and seemingly paradoxical chemical reactivity and physical properties of plutonium (Pu) remains an open question and as such, complicates efforts to predict and rationalize the behavior of Pu in nuclear fuels, solutions, and waste forms. The commitment to resolve this problem was rearticulated and a particular emphasis was placed upon the influence of the 5f electrons in chemical bonding—for example, covalent character, strength, and reactivity—and the contributions thereof to material behavior.

Actinide hybrid materials

Our research addresses this challenge by examining the synthesis and structural characterization of crystalline actinide-containing hybrid materials, i.e., those comprised of organic and inorganic components bonded on the molecular level. The focus on crystalline hybrids containing uranium (U), neptunium (Np), and Pu ensures that structural relationships can be determined crystallographically to establish periodic trends across families of materials. In particular, we have prepared so-called supramolecular hybrids, wherein discrete inorganic and organic building units are assembled into ordered crystalline arrays via non-covalent interactions (NCIs) such as hydrogen or halogen bonds (Fig. 1). Supramolecular assembly requires a reproducible portfolio of actinide-containing building units; this presents a challenge in and of itself owing to metal-ion hydrolysis- and radiolysis-driven redox chemistry, common in aqueous Pu systems. Low-temperature synthesis in aqueous, high-chloride media however effectively reduces speciation diversity. This approach has yielded redox-stable $[AnO_2Cl_4]^{2-}$ anions (An = U, Np, Pu) from aqueous media in which their assembly is directed by charge-balancing and NCI-donating 4-halopyridinium cations, $4XPyH^+$ (X = Cl, Br, I; Fig. 1c).

[1] *Pacific Northwest National Laboratory, Richland, WA 99352;* [2] *The George Washington University, 2121 I St NW, Washington, DC 20052.*

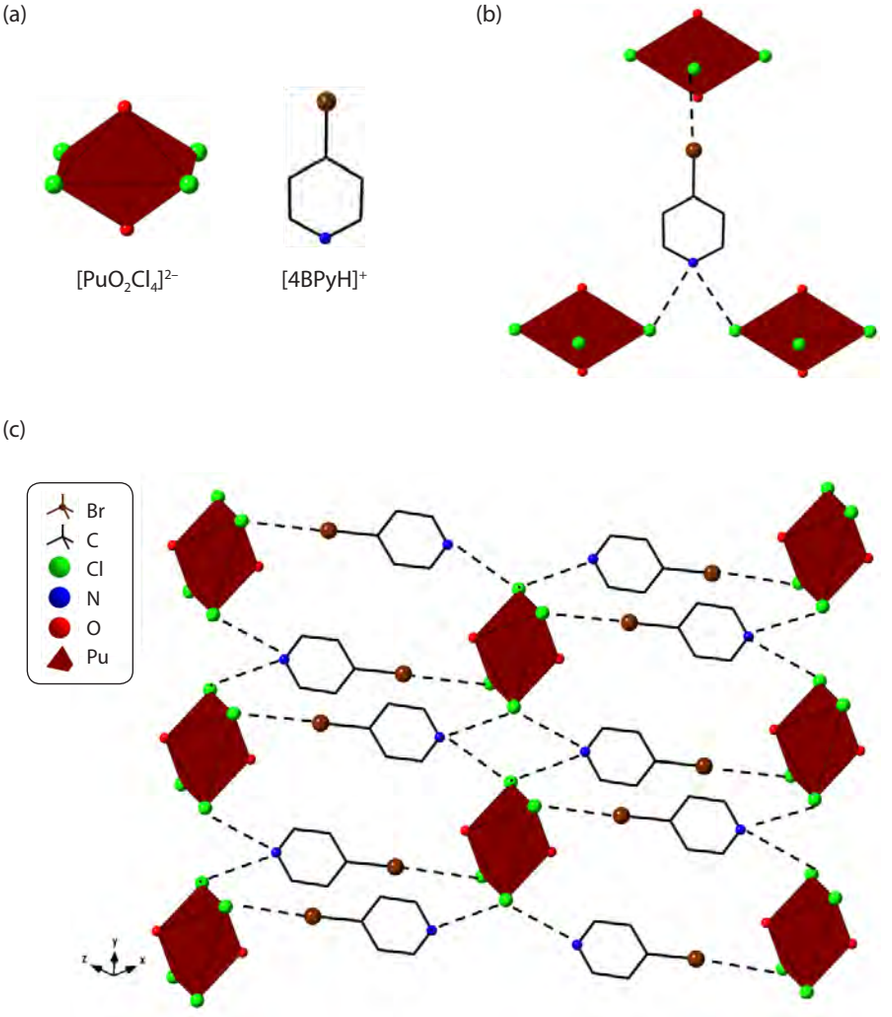

Figure 1. (a) Examples of inorganic and organic building units. (b) The building units are linked via hydrogen and halogen bonds (dashed lines) donated by the $4BrPyH^+$ cations. The Pu atoms are drawn as dark red polyhedra whereas spheres represent oxygen (red), nitrogen (blue), and chloride (green) atoms. The carbon atoms are represented as solid, black sticks and the hydrogen atoms have been omitted here and throughout this article for clarity. (c) Hydrogen and halogen bonds assemble the $[PuO_2Cl_4]^{2-}$ anions in $(4XPyH)_2[PuO_2Cl_4]$ (X = Br, I) into two-dimensional supramolecular sheets.

Structural discussions

Looking comprehensively at the resulting family of 12 compounds when $[AnO_2Cl_4]^{2-}$ anions are paired with $4XPyH^+$ (X = H, Cl, Br, I) cations, we note the formation of only four distinct structure types. One may therefore ask, "Why are the U, Np, and Pu compounds all behaving similarly?" We approached this question computationally, as careful analysis of the electrostatic surface potential of each $[AnO_2Cl_4]^{2-}$ anion revealed that both their magnitude and distribution is invariant across the chlorido ligands (the 'acceptor' sites that receive the NCIs from the $4XPyH^+$ cation 'donors', Fig. 2). Accordingly, the resulting structure type is not influenced by the identity of the metal center, but rather by the nature of the NCI-donating cation. Khon-Sham density functional theory (KS-DFT) calculations support this conclusion as the results indicate that the strengths of the halogen and hydrogen bonds increase and decrease respectively in the order X = Cl, Br, I. Whereas the motivation for this study was admittedly structural in nature, the outcome gave complementary experimental and computational metrics for exploring structure-property relationships across various compositions. More importantly, the reproducibility and generality of the synthetic strategy across the 5f block allows one to generate libraries of related materials, e.g., $(4XPyH)_2[AnO_2Cl_4]$ (An = U, Np, Pu ; X = H, Cl, Br, I, CH_3, OH, NH_2), that are ripe for targeted computational and experimental analyses to probe the influence of 5f electrons on bonding and molecular structure.

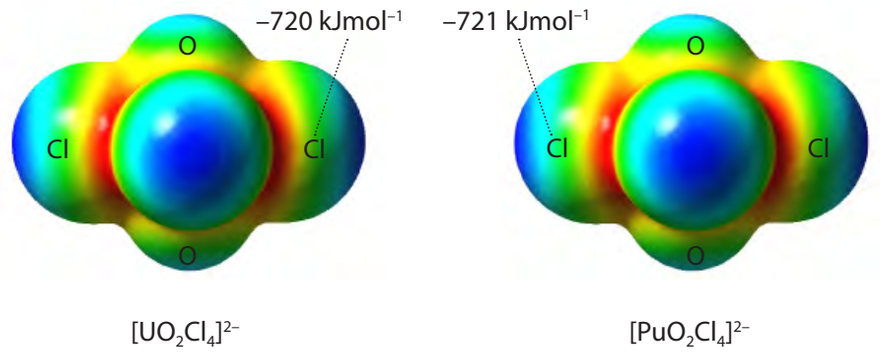

$[UO_2Cl_4]^{2-}$ $[PuO_2Cl_4]^{2-}$

Figure 2. The electrostatic potential of the $[UO_2Cl_4]^{2-}$ and $[PuO_2Cl_4]^{2-}$ anions mapped onto a 0.001 au isodensity surface. The average potential at the Cl acceptor site varies by ~2 kJ mol^{-1} when the metal center is changed U → Np → Pu. The color scale ranges from dark blue to red, which represents potentials of –652 and –786 kJ mol^{-1}, respectively. Adapted with permission from our 2017 publication in the Journal of the American Chemical Society.

Computational approach and discussion

Equipped with a viable synthetic route capable of producing families of related materials as well as a computational workflow, we can systematically probe the electronic structure of Pu by studying its chemical bonds in molecular species. This can be accomplished by leveraging the rather modest suite of crystalline Pu-containing materials we have amassed, as the building units therein, e.g., $[Pu^{III}Cl_3(H_2O)_5]$, $[Pu^{IV}Cl_n(NO_3)^{6-n}]^{2-}$ (n = 0, 2, 3), and $[Pu^{VI}O_2Cl_3(NO_3)]^{2-}$, display a variety of coordination geometries. Computationally, we used both the Quantum Theory of Atoms in Molecules (QTAIM) approach, which describes the topology (i.e., shape and magnitude) of the electron density between two bonded atoms, and the Natural Localized Molecular Orbital (NLMO) method, useful for quantifying the amount of electron sharing, i.e., covalent character between two coordinated atoms, to elucidate Pu bond character and quantify the relative strengths thereof.

The $(4XPyH)_2[Pu^{IV}Cl_n(NO_3)^{6-n}]^{2-}$ (n = 0, 2, 3) series, for example, features ligands that are relevant to separations and disposition chemistries (e.g., NO_3^- and Cl^-) and accordingly, studying the nature of the Pu–NO_3 and Pu–Cl bonds is of both practical and fundamental importance. QTAIM analysis revealed that these bonds are polar and dominated by ionic contributions. Looking more deeply, the analysis also revealed that the strength of the Pu–Cl bond (and the limited covalent character) increases in the order $[Pu(NO_3)_6]^{2-}$ < $[PuCl_3(NO_3)_3]^{2-}$ < $[PuCl_4(NO_3)_2]^{2-}$, with the opposite trend being true of the Pu–NO_3 bonds (in which we note no covalent character was detected, Fig. 3). The results of the NLMO analysis are consistent with those of QTAIM, and in addition provide a means to characterize the hybrid atomic orbitals (HAOs)—those which comprise the bonds—of both the Pu and Cl atoms. The primary orbital constituent of the Pu–Cl bond is the Cl HAO, which speaks to the polar and ionic nature of the bond; on the Pu side, the HAO is composed of mixed s (17%), d (50%), and f (34%) orbital character. Analysis on the atomic orbital level is important as it provides a metric to quantify the f electron contribution in each Pu bond, and moreover the covalency and relative orbital contributions thereof.

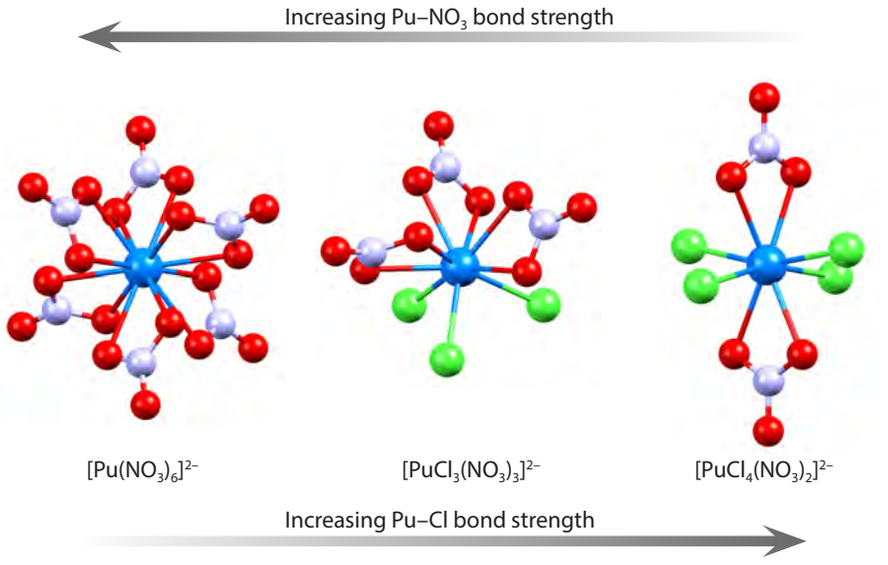

Figure 3. The strength of the Pu–Cl and Pu–NO_3 bonds follow opposite trends. Pu = orange, Cl = green, O = red, N = silver-blue.

Summary

Beyond the structural implications of this work—which are noteworthy in and of themselves as the crystal chemistry of Pu is woefully underexplored relative to the rest of the periodic table—the major takeaway is that the systematic synthetic approach and expanding library of compounds provides a platform to study the fundamental properties and electronic structure of Pu. This not only addresses the current needs of the actinide community, but is also well aligned with the mission of the U.S. Department of Energy with respect to energy, the environment, and national security.

Acknowledgments

The primary source of support for this research was the U.S. Department of Energy (DOE)–Chemical Sciences, Geosciences and Biosciences Division, Office of Basic Sciences, Office of Science, Heavy Elements Program, under grant DE-FG02-05ER15736 at GWU. Computations were carried out by Lucas C. Ducati (University of São Paulo) and Jochen Autschbach (State University of New York at Buffalo) with support from the DOE Heavy Elements Program grant DE-SC0001136. LCD is grateful for fellowships from the São Paulo Research Foundation (FAPESP) 2015/08541-6 and 2017/17750-3. RGS acknowledges support from the National Technical Nuclear Forensic Center and is grateful for the support of the Linus Pauling Distinguished Postdoctoral Fellowship program as a portion of this research was conducted under the Laboratory Directed Research and Development Program at PNNL, a multi-program national laboratory operated by Battelle for the U.S. DOE.

Further Reading:

1. *Surbella III, R. G. and C. L. Cahill (2016). Hybrid materials of the f-Elements Part 2: The Uranyl Cation. Handbook on the Physics and Chemistry of Rare Earths. J. C. Bünzli, G. and V. K. Pecharaky. Amsterdam, Elsevier. 48: 163-285.*
2. *Surbella III, R. G., et al. (2017). "Transuranic Hybrid Materials: Crystallographic and Computational Metrics of Supramolecular Assembly." Journal of the American Chemical Society 139(31): 10843-10855.*
3. *Surbella, R. G., et al. (2018). "Plutonium chlorido nitrato complexes: ligand competition and computational metrics for assembly and bonding." Chemical Communications 54(85): 12014-12017.*

2018 Postdoctoral Publication Prize in Actinide Science
Dr. Patrick Jaffke

Patrick Jaffke

Dr. Jaffke is now a staff member of the Institute for Defense Analyses (IDA) at LANL. He was a summer student in 2014 and a postdoctoral researcher 2017–2018, during which time he was mentored by Patrick Talou (XCP-5: Materials and Physical Data).

On February 7, 2019, the Los Alamos National Laboratory (LANL) G.T. Seaborg Institute hosted a colloquium for Dr. Patrick Jaffke, the 2018 winner of the Postdoctoral Publication Prize in Actinide Science. Dr. Jaffke won the prize for his postdoctoral publication entitled, "Hauser-Feshbach fission fragment de-excitation with calculated macroscopic-microscopic mass yields" published in Physical Review C in 2018 (Phys. Rev. C 2018, 97, 034608). During the colloquium, Dr. Jaffke received a plaque for his prestigious award and a monetary prize. For the attendees, Dr. Jaffke's mentor, Patrick Talou (XCP-5: Materials and Physical Data), provided a brief description of his nomination and highlighted the significance and impact of the awarded work to nuclear science.

The Postdoctoral Publication Prize in Actinide Science, created and funded by Laboratory Fellow Jaqueline L. Kiplinger, is administered by Mary Ann With of the Laboratory's Postdoctoral Program Office in recognition of high impact theoretical or experimental research in fundamental and applied areas of actinide science at LANL. This award is competed and presented to the postdoctoral nominee whose actinide science article describes work performed during the tenure of the postdoctoral appointment at the Laboratory. The successful candidate must be nominated by mentor or other technical staff member who provides a nomination package that highlights the significance and impact of the work, both internal and external, within the field of expertise. Furthermore, the nomination must be approved by group and division management.

Dr. Jaffke presented on the title, "Towards a fully theoretical description of fission". The talk described how nuclear fission begins with the deformation of a nucleus until it typically separates into two nascent fragments. This process can be described as an evolution in a potential energy landscape and has seen a resurgence in theoretical effort over the past 20 years. Next, these nascent fragments de-excite through the emission of prompt neutrons and gamma-rays; a process that can be described in the Hauser-Feshbach statistical formalism. Typically, these fission processes have been examined separately, but in this work Dr. Jaffke presented a combination of the macroscopic-microscopic description of shape evolution and Hauser-Feshbach statistical decay of the produced fragments. This combination provides a more fully theoretical description of fission and provides insight into model sensitivities to experimental observables. Dr. Jaffke and his collaborators demonstrated the effectiveness with two well-studied fission reactions: $^{235}U(n_{th}, f)$ and $^{239}Pu(n_{th}, f)$, finding that the prompt neutron multiplicity can constrain the primary fragment distribution.

Laboratory Fellow Jaqueline L. Kiplinger and the G.T. Seaborg Institute strongly encourage the LANL technical staff and mentorship to nominate postdoctoral researchers for their work in actinide science. It is through such interactions that the Laboratory develops talent and career advancement in this critically important and mission relevant research area.

2018 Postdoctoral Publication Prize in Actinide Science.
Left to right: Franz Freibert, Jaqueline Kiplinger, Patrick Jaffke, and Patrick Talou.

Actinide Research Quarterly is published by Los Alamos National Laboratory and is a publication of the Glenn T. Seaborg Institute for Transactinium Science, a part of the National Security Education Center. ARQ (est. 1994) highlights research in actinide science in such areas as process chemistry, metallurgy, surface and separation sciences, atomic and molecular sciences, actinide ceramics and nuclear fuels, characterization, spectroscopy, analysis, and manufacturing technologies.

LA-UR 19-26103

Address correspondence to:
Actinide Research Quarterly
c/o Editor
Mail Stop T-001
Los Alamos National Laboratory
Los Alamos, NM 87545

ARQ can be read online at:
www.lanl.gov/arq

If you have questions, comments, suggestions, or contributions, please contact the ARQ staff at:
arq@lanl.gov

National Security Education Center
David L. Clark, Director

G. T. Seaborg Institute for Transactinium Science
Science Advisors
Franz Freibert, Director (Acting)
Ping Yang, Deputy Director (Acting)

Editor
Owen Summerscales

Contributing editors
Susan Ramsay

Designers/Illustrators
Don Montoya
Owen Summerscales

Photographer
Mick Greenbank

Circulation Manager
Susan Ramsay

Los Alamos
NATIONAL LABORATORY
EST. 1943

NNSA